Medical Image Analysis 68 (2021) 101905

Contents lists available at ScienceDirect

Medical Image Analysis

journal homepage: www.elsevier.com/locate/media

Survey Paper

A review of machine learning methods for retinal blood vessel segmentation and artery/vein classification

Muthu Rama Krishnan Mookiah[a,*], Stephen Hogg[a], Tom J MacGillivray[b], Vijayaraghavan Prathiba[c], Rajendra Pradeepa[c], Viswanathan Mohan[c], Ranjit Mohan Anjana[c], Alexander S. Doney[d], Colin N.A. Palmer[d], Emanuele Trucco[a]

[a] VAMPIRE project, Computing (SSEN), University of Dundee, Dundee DD1 4HN, UK
[b] VAMPIRE project, Centre for Clinical Brain Sciences, University of Edinburgh, Edinburgh EH16 4SB, UK
[c] Madras Diabetes Research Foundation and Dr. Mohan's Diabetes Specialities Centre, Gopalapuram, Chennai 600086, India
[d] Division of Population Health and Genomics, Ninewells Hospital and Medical School, University of Dundee, Dundee, DD1 9SY, UK

ARTICLE INFO

Article history:
Received 7 June 2019
Revised 10 November 2020
Accepted 11 November 2020
Available online 17 November 2020

Keywords:
Medical imaging
Retinal vessels
Segmentation
Machine learning
Deep learning
Review

ABSTRACT

The eye affords a unique opportunity to inspect a rich part of the human microvasculature non-invasively via retinal imaging. Retinal blood vessel segmentation and classification are prime steps for the diagnosis and risk assessment of microvascular and systemic diseases. A high volume of techniques based on deep learning have been published in recent years. In this context, we review 158 papers published between 2012 and 2020, focussing on methods based on machine and deep learning (DL) for automatic vessel segmentation and classification for fundus camera images. We divide the methods into various classes by task (segmentation or artery-vein classification), technique (supervised or unsupervised, deep and non-deep learning, hand-crafted methods) and more specific algorithms (e.g. multiscale, morphology). We discuss advantages and limitations, and include tables summarising results at-a-glance. Finally, we attempt to assess the quantitative merit of DL methods in terms of accuracy improvement compared to other methods. The results allow us to offer our views on the outlook for vessel segmentation and classification for fundus camera images.

1. Introduction

Non-invasive examination of retinal blood vessels using fundus photography provides accessible information pertaining to vascular health of the eye, body and brain (Vostatek et al., 2017; MacGillivray et al., 2014). Several studies have shown significant associations between structural changes in the retinal vasculature and systemic diseases, including diabetic retinopathy (DR) (Yau et al., 2012), glaucoma (Fraz et al., 2012b), age-related macular degeneration (Fraz et al., 2012b), hypertension (Wong et al., 2001), stroke (Doubal et al., 2008), and cardiovascular diseases (Wong et al., 2001). Increases in vessel width and tortuosity are associated with retinopathy of prematurity and hypertensive retinopathy (Cheung et al., 2011; Sutter and Helbig, 2003). The arteriolar-venular width ratio (AVR) and arteriovenous nicking have been implicated in hypertension and cardiovascular diseases (Smith et al., 2004; Wong et al., 2003; Wong and Mitchell, 2007). Manual segmentation of blood vessels from fundus images is however an exceedingly time-consuming task. Automated vessel segmentation has been investigated for many years, with increasing accuracy, speed and reproducibility (Srinidhi et al., 2017). Automated and semi-automated applications have been also developed for disease screening programs (Mookiah et al., 2013), surgery planning (Kanski and Bowling, 2011), localization of fovea and optic disk (Li and Chutatape, 2004), identification of bifurcation points used for image registration (Zana and Klein, 1999), and biometric identification (Köse et al., 2011).

In the past twenty years, numerous research studies have been conducted on the development of retinal vessel segmentation from fundus images (Srinidhi et al., 2017). Several review papers have covered segmentation algorithms for vessel-like structures in medical images (Felkel et al., 2001; Bühler et al., 2004; Kirbas and Quek, 2004) and automated detection of DR (Mookiah et al., 2013; Patton et al., 2006; Winder et al., 2009; Teng et al., 2002; Abràmoff et al., 2010; Faust et al., 2012). Semi and fully automated methods were reported with comparable segmentation accuracy to human annotators (Fraz et al., 2012b; Srinidhi et al., 2017; Mookiah et al., 2013). Only a limited number of papers have reviewed

* Corresponding author.
E-mail address: mrkmookiah@dundee.ac.uk (M.R.K. Mookiah).

https://doi.org/10.1016/j.media.2020.101905
1361-8415/

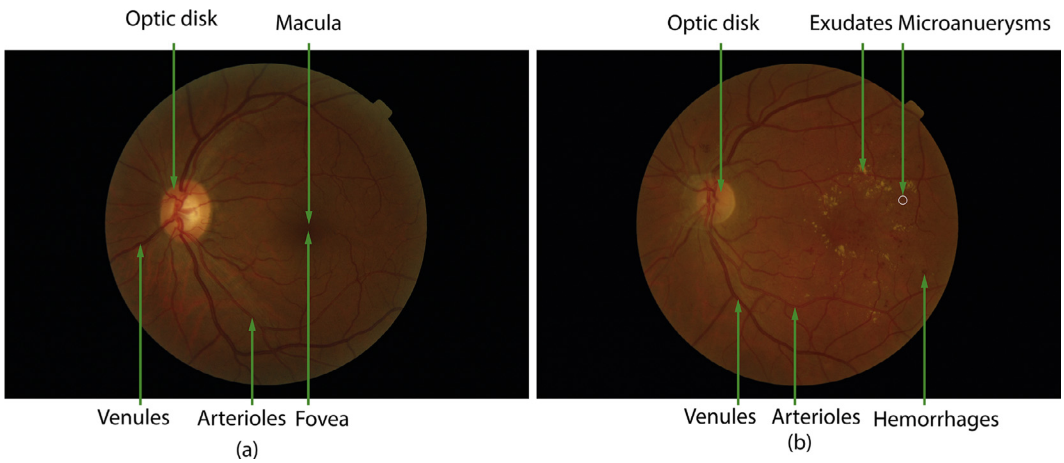

Fig. 1. (a) Normal anatomical structures of the retina (from MESSIDOR); (b) Pathological lesions of DR (from MESSIDOR).

developments in retinal vessel segmentation (Fraz et al., 2012b; Srinidhi et al., 2017); for instance, Fraz et al. (2012b) reviewed blood vessel segmentation algorithms and compared their performance using the well-known public databases DRIVE (Staal et al., 2004) and STARE (Hoover et al., 2000). A brief but recent survey on retinal vessels segmentation is presented by Srinidhi et al. (2017) focussing on preprocessing algorithms, a comparison of state-of-the-art segmentation methods and their performance.

In this survey, we review retinal vessels segmentation and artery/vein classification methods based on machine and deep learning (DL) for fundus photography images published since years 2012. Machine learning, and especially DL in recent years, have established themselves as the dominant paradigm for retinal (and medical in general) image processing. Here we aim to *identify the current challenges and discuss the advantages and limitations of the current approaches. For completeness and to allow comparisons, we include recent methods not using machine learning.* We focus on fundus camera images (Section 2.1) as they remain the most common and important modality for clinical examinations of the retina. We note that optical coherence tomography (OCT) is becoming increasingly widespread, with major optometrist chains in the UK, for instance, now offering such scans to their customers as part of routine health care. For a recent overview of retinal OCT processing techniques we refer the reader to Sonka and Abràmoff (2016); McConnell et al. (2017).

This paper is organized as follows. Section 2 introduces briefly retinal fundus photography and the needs and challenges of retinal vessel segmentation. We present our search protocol, inclusion and exclusion criteria in Section 3. The different types of retinal vessel segmentation and artery/vein classification methods are presented in Section 4 and Section 5. The performance of different retinal vessel segmentation methods are presented in Section 6 and their advantages and limitations in Section 7. A discussion and our conclusions are given in Section 8.

2. Retinal image processing

2.1. Fundus imaging

Fundus imaging captures the main anatomical structures of the retina, namely the optic disk, macula, fovea, and blood vessels (Fig. 1a). Pathological changes (some of which are illustrated in Fig. 1b) in these structures and elsewhere in the retina signal different eye diseases (Mookiah et al., 2013) and have also been associated with the risk, onset and progression of a variety of systemic diseases (Li et al., 2018; McKay et al., 2018). The retina is imaged via a low-power microscope and camera attachment (Srinidhi et al., 2017; Mookiah et al., 2013) or a laser device (Webb and Hughes, 1981). The optics are similar to those of an indirect ophthalmoscope to provide a magnified view of the inner surface of the eye. The main fundus imaging techniques are color fundus photography, fluorescein angiography (FA), and scanning laser ophthalmoscopy (SLO), depending on the instrument (and allied acquisition protocol). The FA examination involves injecting the patient with fluorescein dyes and acquiring sequences of images to study the flow of blood, obstructed vessels and points of leak. SLO uses laser scanning, which provides high-contrast images of the vasculature (Srinidhi et al., 2017; Mookiah et al., 2013) and is used in wide-field-of-view instruments (Pellegrini et al., 2014; 2018; Csincsik et al., 2017).

For a recent, detailed introduction to retina imaging we refer the reader to Trucco et al. (2019).

2.2. Challenges in retinal vessel segmentation

The performance of retinal vessel segmentation methods reported in papers is often close to that of human observers (Fraz et al., 2012b; Srinidhi et al., 2017; Mookiah et al., 2013) given the test sets and assessment criteria. Neither, and especially the latter, is however consistent across papers, a limit affecting medical image analysis in general (notice that the international debate on the validation of algorithms and the design of international challenges is stepping up (Galdran et al., 2018; Zhao et al., 2018b; Zhang and Chung, 2018; Wu et al., 2018)).

Several factors make reliable segmentation of the full retinal vasculature a challenge for image processing. The major ones can be summarized as follows (Fraz et al., 2012b; Srinidhi et al., 2017).

i Central light reflex causing a gap in the segmented vessel which creates *two* smaller ones in the segmentation map (Fig. 2a).
ii Poorly contrasted small vessels that are missed by the segmentation (Fig. 2b).
iii Broken vessels at bifurcations/crossover points (Fig. 2c).
iv Close, parallel vessels segmented as a single large one (Fig. 2c).
v Imaging artefacts (e.g. noise, non-uniform illumination, blur) (Fig. 2d).
vi Lesions (microaneurysm, exudates, cotton wool spots, haemorrhages, neovascularization) generating false positives, or obscuring or disrupting blood vessels (Fig. 1b).

Meeting the above challenges is crucial to achieve a stable, repeatable and high accuracy over independent data sets acquired with different instruments, protocols, operators and patient cohorts, and ultimately to enable reliable translation of research

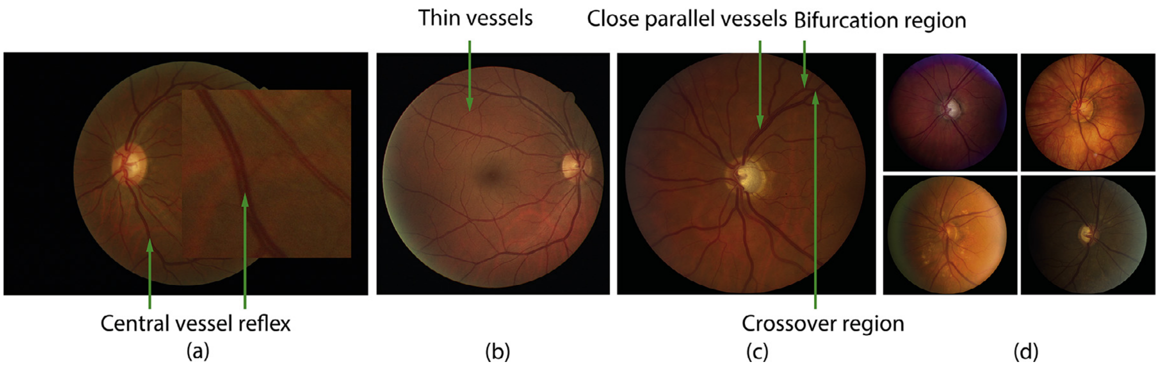

Fig. 2. Retinal images with (a) the presence of CVR (from MESSIDOR); (b) Thin vessels (from DRIVE); (c) Close parallel vessels (from INSPIRE-AVR); (d) Imaging artefacts (from INSPIRE-AVR).

techniques to healthcare. Recent deep learning methods achieve excellent performance on vessel segmentations (Fu et al., 2016a; Zhou et al., 2017; Liskowski and Krawiec, 2016; Yan et al., 2018b) when tested on standard, public data sets, typically DRIVE or STARE, composed of modest numbers of images with ground truth. This important point is discussed in Sections 6 and 7. We notice that this limitation is gradually changing; see e.g. the REFUGE challenge at MICCAI 2018 created a data set of 1200 images with annotations for the two target tasks, namely optic disc/cup segmentation and glaucoma detection. This data set was reported in a MedIA paper (Orlando et al., 2019).

3. Methodology

3.1. Material sourcing

Journal and conference papers on retinal vessel segmentation techniques and classification published between 2012 to 2020 were sourced from PubMed, Web of Science, IEEE Xplore, and Google Scholar. The search terms were "retinal imaging," or "fundus photography," or "vessel segmentation," or "artery/vein classification," or "retinal vasculature," or "matched filter," or "Gaussian filter," or "hysteresis thresholding," or "vessel enhancement," or "machine learning," or "deep learning". The search filters were applied to date, keywords, title, and abstract. Before filtering, there were more than 500 hits, reduced to 240 after filtering, of which 19 published in 2019 or 2020. The inclusion and exclusion criteria (next section) were applied to this set.

3.2. Inclusion/exclusion criteria

The inclusion criteria were (i) original study; (ii) written in English; (iii) vessel segmentation methods using fundus imaging; (iv) retinal artery/vein classification or retinal vessel segmentation; (v) evaluated on public and private databases, or public databases.

The exclusion criteria were (i) review studies; (ii) non-English language studies; (iii) conference abstracts; (iv) studies focused only on specific vascular properties or structures, e.g. arteriovenous nicking, major vessel width and bifurcation measurements. This step resulted in a final collection of 158 papers. The criteria were applied by checking the full paper contents.

4. Retinal vessel segmentation methods

In this section we review recent retinal vessel segmentation methods for color fundus, FA and SLO images. Machine learning methods are classified into supervised and unsupervised ones, forming the majority of this section. Recent, non-ML methods are included for comparison and completeness, and organized by technique into (i) morphological image processing, (ii) vessel tracing/tracking, (iii) multi-scale, and (iv) other methods. Each category is discussed separately and the papers included summarized in table form in the Appendix. For each paper entry, the tables specify authors, date of publication, key algorithms adopted (methods), validation databases, segmentation challenges addressed from the list in Section 2.2, and performance (incl. criteria and figures). A paper can feature in multiple sections if falling into multiple categories.

4.1. Machine learning methods

Machine learning methods are further divided into supervised and unsupervised (Fraz et al., 2012b; Srinidhi et al., 2017; Mookiah et al., 2013). Supervised methods use images together with ground truth labels to train classification models. Beyond DL methods, we include Bayesian methods, discriminant analysis, k-nearest neighbour (kNN), support vector machine (SVM), artificial neural network (ANN), random forest, AdaBoost, and fuzzy techniques (Fraz et al., 2012b; Srinidhi et al., 2017; Mookiah et al., 2013). Unsupervised methods, including Gaussian mixture model (GMM), fuzzy c-means (FCM), and *k*-means clustering performs vessel segmentation without training labels.

4.1.1. Deep learning

An appealing property of DL models like convolutional neural network (CNN)s is their ability to compute representations relevant for classification and categorization.

CNN for vessel segmentation have been used *per se* (Maninis et al., 2016; Guo et al., 2018) as well as in combination with random forests (Wang et al., 2015; Maji et al., 2015) or conditional random fields (CRF) (Fu et al., 2016b). Modified architectures including specialized layers have been reported, for instance, for integrated vessel-optic disk detection (Tan et al., 2017; Maninis et al., 2016; Jiang et al., 2018), pre-trained with millions of natural images. The CRF layers model long-range interactions between pixels and have been reported to improve the segmentation of various lesions (Fu et al., 2016a; 2016b; Luo et al., 2016).

Dense CRF models (Liskowski and Krawiec, 2016; Zhou et al., 2017; Oliveira et al., 2018), some of which including reinforcement sample learning to reduce training time (Dasgupta and Singh, 2017), were used successfully for thin vessel segmentation, one of the challenges for conventional techniques.

Finally, fully convolutional network (FCN) have been reported to improve vessel segmentation results compared to networks using only some fully connected layers (Brancati et al., 2018; Meyer et al., 2017; Yan et al., 2018b; 2018a; Hu et al., 2018). Multiple networks have been combined to reduce the volume of training examples (Mo and Zhang, 2017; Xu et al., 2018) and achieve multi-scale analysis, for instance integrating the outputs of width-specific vessel detectors (Yan et al., 2018b) or building a wavelet transform into the model (Oliveira et al., 2018). generative adversarial nets (GANs), typically used for generating synthetic retinal images, have been exploited for training, boosting segmentation performance e.g. in the presence of lesions (Zhao et al., 2018a; Park et al., 2020).

The summary of vessel segmentation using DL is presented in Table A.1.

4.1.2. Other machine learning methods

Supervised Methods

Backpropagation neural networks (NN) have been used widely in retinal vasculature segmentation, sometimes in combination with texture (Rahebi and Hardalaç, 2014), color (Franklin and Rajan, 2014), intensity (Vega et al., 2015; Fraz et al., 2014) and moment invariant features (Vega et al., 2015). Lattice NN with a single layer feed forward have been shown to improve convergence (Vega et al., 2015). Wide and deep NN with cross-modality learning have been adopted for vessel segmentation with noisy images presenting signs of pathologies (Fathi and Naghsh-Nilchi, 2014). Feature descriptors like local binary patterns (LBP) and various shape features have been used with NN to segment thin vessels (Kaur and Mittal, 2017; Fathi and Naghsh-Nilchi, 2014).

Gaussian, Wavelet, and Gabor filters have been combined with intensity, Hessian-based and scale invariant feature transform (SIFT) features for vessel enhancement and segmentation using NN and linear discriminant analysis (LDA) (Cao et al., 2012; Shah et al., 2017; Zhang et al., 2015; Condurache and Mertins, 2012). SCIRD-TS filters, a learnt battery of parameterized Gaussian filters with curvilinear support, were used successfully for thin vessel segmentation (Annunziata and Trucco, 2016).

Ensemble learning algorithms like bagging and boosting methods have been tried togeter with intensity, texture, and Gabor features for vessel/non-vessel pixel classification (Fraz et al., 2012c; Memari et al., 2017; Fraz et al., 2014; GeethaRamani and Balasubramanian, 2016; Schapire and Singer, 1999). B-COSFIRE and Frangi filters were used to enhance vessels (Memari et al., 2017). Features identified by the well-known AdaBoost algorithm, building a classification model from a linear combination of weak classifiers, have been shown to encode vessel information from normal and pathological pediatric retinal images (Fraz et al., 2014; Schapire and Singer, 1999).

Fuzzy inference has been tried with multi-scale LBP, Gaussian, and directional features (Fathi and Naghsh-Nilchi, 2013b; Sigurðsson et al., 2014). Sparse representation classifier with dictionary learning (Zhang et al., 2012; Javidi et al., 2017), ensemble features with divergence vector field (Zhu et al., 2017; 2016) and classifier fusion have all been reported to imrpove resilience to clutter (e.g. lesions) inwith pathological images (Barkana et al., 2017; Kalaie and Gooya, 2017).

SVM have been combined with fully connected conditional random field to addressed poor segmentation problems associated with weak priors. Here, each pixel was considered as a feature extracted through gradient magnitude and matched filtering (MF) response (Orlando et al., 2017b; Orlando and Blaschko, 2014; Orlando et al., 2017a). Shape and intensity features showed improved vessel segmentation with lesions (Ganjee et al., 2014; Waheed et al., 2015; Tang et al., 2017) and closely parallel vessels were removed using *k*-means clustering and SVM (Panda et al., 2016). Binary Hausdorff symmetry measure, Gabor, B-COSFIRE filters and multi-fractal features joint with SVM also reported resilient vessel segmentation in the presence of lesions (e.g. DR, hypertensive retinopathy) (Panda et al., 2016; Ding et al., 2015; Strisciuglio et al., 2016; Jebaseeli et al., 2019). Visual attention modelling were used in random forest classifiers to handle images with the challenges posed by close parallel vessels, CVR, low-contrast thin vessels, lesions, and non-uniform illumination (Cheng et al., 2014; Srinidhi et al., 2018).

The summary of vessel segmentation using supervised methods other than DL is presented in Table A.2.

Unsupervised Methods

The main advantage of unsupervised vessel segmentation methods is that they do not need manual annotation (ground truth or gold standard). They use or discover image properties leading to grouping pixels into vessel and non-vessel.

The GMM-expectation maximization (EM) algorithm was also used for vessel segmentation. EM provided a maximum-likelihood vessel/non-vessel pixel classification, with vessel enhancement performed by high-pass filtering and top-hat transform (Roychowdhury et al., 2015a). Combined GMM and Gray voting allowed integrated optic disk and vessel segmentation, with Gabor filtering containing vessel fragmentation and improving thin vessel segmentation (Roychowdhury et al., 2015a; Dai et al., 2015).

FCM clustering was tried with a weighted combination of filters (matched, Frangi's, and Gabor wavelets) for thin vessel enhancement and blob removal from fundus images (Oliveira et al., 2016; Emary et al., 2017; Hassanien et al., 2015). Evolutionary approaches like bee colony optimization have been directed to identify vessel clusters and texture-based spatial dependence probabilities to separate vessel pixels from background (Neto et al., 2017; Hassan and Hassanien, 2018).

The summary of vessel segmentation using unsupervised methods is presented in Table A.3.

4.2. Matched filtering methods

MF is a classic template matching technique (Chaudhuri et al., 1989), indeed so widespread and still used as baseline sometime to deserve a brief section. MF convolves retinal images with predefined kernels modelling the intensity profiles of vessels. It assumes that vessels are locally linear in shape. Many authors model the cross-sectional intensity profile as a Gaussian, although some have proposed more complex models (Kovács and Hajdu, 2016; Singh and Srivastava, 2016; Liu et al., 2016). MF-filtered images are thresholded with a variety of techniques (e.g. hysteresis, Kittler minimum error) to obtain the final binary vessel map (Chaudhuri et al., 1989).

Intensity clipping and directional filters were used to enhance vessels from narrow to wide (Ramlugun et al., 2012; Odstrcilik et al., 2013). The curvelet transform and Laplacian-of-Gaussian filter were used to enhance thin and low-contrast vessels from images with lesions and bright blobs and to discriminate thick, medium, and thin vessels (Kar and Maity, 2016a; 2016c; 2016b).

2D Gabor, multi-scale line, anisotropic diffusion and B-COSFIRE filtering (Tan et al., 2016; Singh and Srivastava, 2016; Soomro et al., 2017; Liu et al., 2016) have also been reported to enhance vessels, with SVM obtaining the final segmentation using contrast and diffusion maps (Liu et al., 2016). Spline fitting was used to edit the vessel segmentation (Tan et al., 2016) and length and adaptive filtering to remove artefacts (Rezaee et al., 2017; Liu et al., 2016). Automatic parameter tuning for Gabor filters (Kovács and Hajdu, 2016) has been reported with particle swarm optimization (PSO) (Subudhi et al., 2016) and “imperialism competitive algorithm” (ICA) (Farokhian et al., 2017). Finally, MF was also tried with a portable FPGA-based hardware architecture (Koukounis et al., 2014; Krause et al., 2016).

The summary of vessel segmentation using matched filtering is presented in Table A.4.

4.3. Morphological image processing methods

Digital image processing mathematical morphology detect boundaries, skeletons, and convex hulls (Haralick et al., 1987; Gonzalez and Woods, 2007). Morphological operators such as dilation and erosion were used as structuring elements to fill holes, connect disjoint regions and shrink the objects in binary images (Serra, 1979). Generally, the top-hat transformation has been very popular to enhance vessels, by estimating the image background using morphological opening operations (Fraz et al., 2012b; Badsha et al., 2013).

Multi-directional morphological top-hat transform, H-maxima transform, and bit plane slicing were used for vessel enhancement (Fraz et al., 2013; 2012a; Saleh and Eswaran, 2012), first order derivative of Gaussian (FoDoG) and iterative region growing were used to segment vessel centerline and final binary map obtained using multilevel thresholding (Saleh and Eswaran, 2012). morphological component analysis (MCA) and morlet wavelet transform (MWT) were successfully used to separate vasculature from pathological lesions (Imani et al., 2015). Adaptive thresholding, morphology-based global thresholding and FoDoG were combined for thin vessel detection (Jiang et al., 2017; Imani et al., 2015). Hidden markov model (HMM) was used to trace the vessels and segment thick and thin vessels even with in the presence of occlusion (Hassan et al., 2017). Finally, *mean*-C thresholding, with morphological cleaning were used to discard the disjoint regions to improve the segmentation accuracy (Dash and Bhoi, 2017).

The summary of vessel segmentation using morphological image processing is presented in Table A.5.

4.4. Vessel tracing and tracking methods

Vessel tracing and tracking methods follow vessels starting from seed points typically selected from edges or centerlines. This approach uses local information and often provides vessel widths, connectivity information at the challenging bifurcation and crossover points.

Particle and Kalman filtering were used in combined with hysteresis thresholding to determine vessel and vessel crossing regions (Nayebifar and Moghaddam, 2013; Lin et al., 2012). Vesselness maps were computed using MF over multiple scales and orientations (Yang et al., 2017; Wang et al., 2013a; Sofka and Stewart, 2006). Minimum-cost matching, global graph optimization and Dijkstra's algorithm were adopted to ensure vessel continuity (Nayebifar and Moghaddam, 2013; Lin et al., 2012; Sofka and Stewart, 2006) when segmenting tortuous and low-contrast vessels with retinal photographs of premature infants (Sofka and Stewart, 2006).

Techniques using snakes, gradient directions and minimal paths exploited features extracted from vessel profile to classify vessel segments as arteries and veins by *k*-means clustering (Vázquez et al., 2013). Multi-scale line and orientation detection (Bekkers et al., 2014) adopted for vessel edge and centreline tracking in challenging regions near bifurcation and vessel crossing (Zhang et al., 2014). Frangi filter response (Nergiz and Akın, 2017; Khan et al., 2018) was used to enhance the thin vessel segments, Otsu's thresholding and tensor coloring were used to generate binary vessel maps (Khan et al., 2018).

The summary of vessel segmentation using vessel tracing/tracking is presented in Table A.6.

4.5. Multi-scale methods

Multi-scale methods have been investigated in image processing and computer vision since the 80s (Lindeberg, 2013). The rationale is that large vessels will be best detected at low spatial scales, and thin vessels at high spatial scales, so that each scale allows optimal structure segmentation in the corresponding specific size (vessel width) range.

A multitude of multi-scale techniques have been reported, including MF (Lázár and Hajdu, 2015; Li et al., 2012; Lazar and Hajdu, 2012; Hannink et al., 2014) (in combination with pixelwise directional response, hybrid region growing and one-class kNN), Frangi vesselness with multi-scale Gaussian derivative filters, and orientation scores. In terms of the challenges listed above, multi-scale line detection and double thresholding were used to enhance thin vessels, vessels at crossover points and close parallel ones (Nguyen et al., 2013; Li et al., 2012; Ricci and Perfetti, 2007). Curvature-regularized fast marching and multi-scale vesselness filter responses led to segmentation resilient to high curvature (Liao et al., 2013). Combinations of multi-scale directional filters and differential fusion have been reported to enhance thin vessels and lower the CVR in arteries and veins (Christodoulidis et al., 2016; Pandey et al., 2017; Zhen et al., 2014).

Log-Gabor filter response at different scales (Dizdaro et al., 2012) was used to detect poor contrast and narrow to retinal vessels, improved circular Gabor filter (ICGF) and multidirectional multi-scale second derivation of Gaussian (MMSDG) (Meng et al., 2015) were combined with global thresholding and elongating filters to segment vessels and to discard blobs, and spur regions from the vessel map (Meng et al., 2015; Dizdaro et al., 2012). Multi-scale second-order Gaussian derivative filter response (Pellegrini et al., 2014; Zhang et al., 2017; 2016) and orientation score were used for vessel segmentation, the intensity cross sectional profiles of vessels together with a NN to estimate the likelihood of pixel, the Gaussian derivative filter response handles segmentation at vessel crossings, vessels with CVR, parallel, and thin vessels (Pellegrini et al., 2014; Zhang et al., 2016).

Wavelet sub-bands (Fathi and Naghsh-Nilchi, 2013a; Wang et al., 2013b; Bankhead et al., 2012) were adopted to enhance the thick and thin vessels and an anisotropic Gaussian filter was employed to solve CVR. Multi-wavelet kernels were successfully used to localize central-reflection, microaneurysm (MA), and bright lesions to improve the thin vessel detection (Wang et al., 2013b; Zhao et al., 2014).

Hessian based multi-scale approach (Aslani and Sarnel, 2016; Rodrigues and Marengoni, 2017; Guo et al., 2017; BahadarKhan et al., 2016) was applied to enhance the wide and thin retinal vasculatures, exudate inpainting (Annunziata et al., 2016) was used to reduce false positives and improve retinal vasculature detection. Shearlet transform, multi-Scale Laplacian of Gaussian filter and anisotropic filtering (Soomro et al., 2018; Labate et al., 2005) have shown improved vessel segmentation with pathological images (Soomro et al., 2018; Labate et al., 2005). ICA-based (Soomro et al., 2018) vessel enhancement was used with global, adaptive, and hysteresis thresholding to obtain binary vessel maps (Moghimirad et al., 2012; Wang et al., 2013b; Zhao et al., 2014; Rodrigues and Marengoni, 2017).

The summary of vessel segmentation using multi-scale methods is presented in Table A.7.

4.6. Other methods

This final short section mentions techniques not fitting in the previous categories published in the target time period.

Gaussian processes (Asl et al., 2017) have been used to address the challenges of vessel detection with bifurcations, CVR, and thin vessels, for instance with features computed by the Radon transform (Deans, 2007). Graph cuts and deformable models, such as active contours and level sets (Zhao et al., 2017; 2015b; Salazar-Gonzalez et al., 2014; Dizdaroğlu et al., 2014; Zhao et al., 2015a), local phase vessel enhancement (Zhao et al., 2015a) (for both RGB and FA images) (Zhao et al., 2017; 2015a), iterative vessel segmentation and adaptive global thresholding (Roychowdhury et al., 2015b; Xue et al., 2018) all were reported to improve segmentation variousy, especially in the presence of lesions.

The summary of these methods is presented in Table A.8.

5. Artery/vein classification methods

The number of papers addressing specifically A/V classification in the time period considered is significantly smaller than the ones on vessel segmentation.

Standard CNN have been tried for artery/vein classification and could also segment thin vessels in the presence of occlusion (Welikala et al., 2017). Likelihood graph propagation have proven effective to correct wrongly classified pixels (Girard and Cheriet, 2017; Girard et al., 2019). FCN (U-Net) have also been reported for artery/vein segmentation (Hemelings et al., 2019; Ma et al., 2019). GANs with topological structure constraints with adversarial loss proved efficient capable of capturing pixel-wise features and superior to other methods for learning the probability distribution of the arteriovenous segmentation map (Yang et al., 2020).

LDA was used in combination with intensity, retinex normalization and reflection properties of the vessels for vessel classifiation and AVR estimation (Mirsharif et al., 2013; Dashtbozorg et al., 2014; Huang et al., 2018; Dashtbozorg et al., 2013). The AVR is a ratio of the weighted average width of the arterioles to that of the venules around the optic disc, and a well-known coefficient in retinal biomarkers research (Hemelings et al., 2019). Bayes classifiers and graph cut have been used on ultra-wide field of view (UWFoV)-SLO images (Pellegrini et al., 2018).

Feature-based vessel classification has been tried with various classification and clustering techniques. SVM (Akbar et al., 2018; Vijayakumar et al., 2016; Hu et al., 2015; Vapnik et al., 1995) has been reported with width, orientation, Gabor, intensity and morphological features, including feature selection using random forest (RF), and graph-theoretic frameworks with vessel tree network topology (Estrada et al., 2015a). kNN was tried with multi-scale, color, texture, and adaptive LBP features (Xu et al., 2017; Zhu et al., 2017; Joshi et al., 2014; Zou et al., 2017; Yin et al., 2020), and *k*-means clustering with color features to classify artery/vein in specific fundus image quadrants (Fu et al., 2017) to compute AVR (Relan et al., 2013; 2019). Another classifier tried was JointBoost with vessel network topology (Yan et al., 2017).

Vessel tracing and optimal forest graph representations were incorporated in the well-known system Singapore “i” vessel assessment (SIVA), used in many clinical studies (Lau et al., 2013). Futher techniques include markov random field (MRF) based energy functions (Eppenhof et al., 2015), RF classifiers with Gabor wavelet and statistical histogram features, vessel keypoint detection, and metaheuristic graph search (Srinidhi et al., 2019).

The summary of methods found using DL, supervised, unsupervised, vessel tracing/tracking, and multi-scale methods is presented in Table A.9.

6. Performance summary

This section summarizes the performance levels reported by papers in different techniques groups. We discuss results and issues related to performance in Section 7 (discussion), including the choice of criteria and datasets, and the challenge of a fair and complete comparison among methods. We refer the reader to the tables in the Appendix for a complete list of performance data in each paper reviewed.

Supervised segmentation methods including deep learning. In general, very good performance for vessel segmentation has been achieved by recent deep learning methods, for instance 96.28% segmentation accuracy by a deep and wide NN on STARE for healthy images and 96.72% on STARE and DRIVE for pathological images (Li et al., 2016) (Li et al. (2016); Srinidhi et al. (2018), Table A.2). Reported vessel segmentation accuracies of CNN, again on STARE and DRIVE and in combination pre- or postprocessing, CRF and other techniques, have reached about 98% on the same datasets (Liskowski and Krawiec, 2016).

The level of accuracy is not so high for artery-vein classification. Very few studies reported artery/vein classification with an accuracy greater than 90% (Xu et al., 2017; Akbar et al., 2018; Zhu et al., 2017; Vijayakumar et al., 2016; Estrada et al., 2015a; Relan et al., 2013; Joshi et al., 2014; Huang et al., 2018; Dashtbozorg et al., 2013; Yan et al., 2017; Lau et al., 2013; Eppenhof et al., 2015; Fu et al., 2017; Girard and Cheriet, 2017) using different databases (Table A.9). Recent methods in Pellegrini et al. (2014, 2018); Srinidhi et al. (2018); Meyer et al. (2017) made an attempt to perform segmentation on SLO images with a reported accuracy above 95% (Pellegrini et al., 2014; Srinidhi et al., 2018; Meyer et al., 2017).

Unsupervised clustering. The best accuracy reported by papers on unsupervised clustering with STARE and DRIVE is around 97% (Joshi et al., 2014) for vessel segmentation but only around 92% for vessel classification. Moreover, these methods may fail for images with non-uniform illumination, producing false positives for DR lesions (exudates and haemorrhages) and optic disk (Fraz et al., 2012b).

Matched filtering. These methods have been honed over a very long period of time and, perhaps not surprisingly, have achieved high accuracy on DRIVE and STARE for vessel segmentation. They are not used for vessel classification. A Gabor template matching-method (Kovács and Hajdu, 2016) have reported accuracy of 96.78% on the HRF dataset, more recent than STARE and DRIVE and consisting of healthy, DR, and glaucomatous imagesMulti-resolution techniques have also reached (about 97.06% for healthy and about 95% for pathological images on STARE (Kar and Maity, 2016a). This class of methods *per se* seems unable to cope with lesions, hence MF is often combined with other techniques (Sofka and Stewart, 2006; Cinsdikici and Aydın, 2009).

Mathematical morphology. Reported accuracies for vessel segmentation here are lower than the ones above, hovering around 94% and 96% (Fraz et al., 2012a; Hassan et al., 2017). These methods rely on fixed structuring elements mostly assuming locally linear vessels, which has proven a limit with highly tortuous vessels.

Tracing algorithms. Tracking methods require seed points to detect vessel segments; different initializations may lead to rather different results. Also, failing to detect a bifurcation may imply missing an entire sub-tree. Very high pixelwise precision (98.9%) and recall (98.7%) were reported in Lau et al. (2013) with good resilience to noise but comparison with other methods is complicated by the use of a non-public dataset (Singapore Malay eye study) and the absence of accuracy figures. Tracking based on multi-orientation analysis and orientation scores were used to identify vessels at bifurcations and crossings in Bekkers et al. (2014), achieving accuracies at crossings and bifurcations of 95.61% and 76.12% respectively on the public HRF dataset.

Multi-scale methods. These methods have reported specific successes with the challenges listed in Section 2.2. Locally adaptive derivative filters and scale-orientation scores have been showed to enhance vessel structures at crossings/bifurcations, and to address CVR, close parallel vessels, and low-contrast small vessels, topping vessel segmentation accuracies between up to 97% (Zhang et al., 2017 on STARE, DRIVE and CHASEDB1; Zhang et al., 2016 on multiple datasets including DRIVE, STARE, CHASEDB1, HRF, and UWFoV SLO (Hannink et al., 2014).

Iterative adaptive global thresholding. This technique proved both computationally efficient and quite successful as part of segmentation methods, but never associated with segmentation accuracies above 96% on various data sets.

7. Discussion

It should be clear from the presentation so far that there is no easy way to compare the many methods reported on a fair, common basis. This section addresses the main issues involved and offer some thoughts on the way forward.

7.1. Qualitative observations

The issue of the availability, design and purpose of public datasets is a recognized important part of the wider field of validation of medical image analysis, on which a healthy international debate is increasing (Maier-Hein et al., 2018a; Joskowicz et al., 2019; Trucco et al., 2013; Silberzahn and Uhlmann, 2015). This includes several international grand challenges with well-defined but often different performance criteria. We mention here two examples for retinal image analysis, although not on vessel detection and labelling specifically. One is REFUGE at MICCAI (https://refuge.grand-challenge.org/), linked to the OMIA workshop on retinal image analysis. REFUGE 2018 obtained 1200 images (400 for training) annotated by 7 independent experts; the target problems were OD detection, glaucoma classification, and fovea localization. The other is the IDRiD (Indian DR Image Dataset) challenge at ISBI 2018 (https://idrid.grand-challenge.org/) on DR detection and grading, and diabetic macular edema. There are more, easily located on the web. Very interesting observations based on a quantitative analysis of the results of MICCAI Grand Challenges in recent years are presented in Maier-Hein et al. (2018a).

The majority of retinal vessel segmentation methods reported were evaluated on DRIVE (Staal et al., 2004), STARE (Hoover et al., 2000), CHASEDB1 (Owen et al., 2009), and HRF (Budai et al., 2013). Some methods were evaluated on further datasets, some of which public, some proprietary: MESSIDOR (Decenci'ere et al., 2014), ARIA (Zheng et al., 2012), DIARETDB1 (Kälviäinen and Uusitalo, 2007), REVIEW (Al-Diri et al., 2008), genetics of diabetes audit and research in tayside Scotland (GoDARTS) (Perez-Rovira et al., 2011b), IOSTAR (Zhang et al., 2016), and RC-SLO (Zhang et al., 2016). Artery/vein classification methods reviewed, in turn, were evaluated using VICAVR (Vázquez et al., 2013), INSPIRE-AVR (Niemeijer et al., 2011), and WIDE (Estrada et al., 2015b). STARE, automated retinal image analyser (ARIA), HRF, VAMPIRE, INSPIRE-AVR, and WIDE contain images with lesions (e.g. DR, age-related macular degeneration (AMD), glaucoma) enabling robustness tests against confounders for vessel detection (Section 2.2). IOSTAR and RC-SLO address further segmentation challenges like CVR, thin vessels, and bifurcations/crossover points. Finally, a few more datasets are very small (see Table A.1 to Table A.3) and rarely used. We summarize in Table A.11 the datasets for retinal vessel segmentation and artery/vein classification encountered in our survey. All datasets were developed independently of each other; although all adopt sensible performance criteria and no doubt competent ground truth annotations, the absence of acknowledged international standards is a serious limit to the comparison of competing techniques.

The much smaller number of papers on A/V classification than on vessel segmentation can be explained with three reasons.

First, the applicative need for A/V labelling is mostly felt in clinical statistical studies on the association of the retinal phenotype with clinical outcomes, in which the different circulatory functions of the arterial and venular networks require separate analyses. Not every group publishing on vessel classification is involved in such studies.

Second, public datasets with A/V ground-truth labels remain fewer and less visible than the ones for vessel segmentation (requiring only unlabeled vessel maps).

Third, vessel classification implies vessel segmentation, but not vice versa. Consequently, it has been easier for image analysis groups, especially those new to the field, to tackle vessel segmentation. This situation is now changing with the emergence of DL systems for simultaneous segmentation and classification.

One may wonder whether it has simply become impossible to improve accuracy on DRIVE and STARE, given the annotations provided. We note that the accuracy histogram for DRIVE (Fig. 3 (b)), although clearly concentrated around 95–96%, is also spread from 92% to 98%. This indicates that there is still space to improve (nobody has achieved 100%, although the merit of matching perfectly the annotations of one or two annotators, see below, may be debatable) and that not all techniques achieve the same accuracy (only about 60% of the papers achieve an accuracy in the majority interval).

We also note that, given the annotations in DRIVE, “improve” means “resemble better one or two annotators” only. The authors of DRIVE divided the 40 images provided in two sets of 20 images each, for training and testing respectively. Two manual annotators traced the vasculature in the latter (to provide a reference for the results), but only one in the former. This, in turn, points to the complex issue of designing ground truth, that is still the object of debate in the medical image analysis community. Open questions include what instructions to give the annotators (annotation protocol), how to deal with different annotations, the dependency of the ground-truth design on specific purposes, the number of annotators, and the criteria for evaluation. Again, we refer the reader to the very informative discussion by Maier-Hein et al. (2018b) and references therein.

7.2. Quantitative analysis

Has deep learning shown clear superiority compared to non-DL methods? If we look carefully, the answer is not that straightforward. DL has brought about undisputable breakthroughs in various fields (speech analysis and synthesis, automatic captioning, face and object recognition, retinal patient triage and CVD risk (De Fauw et al., 2018)). Here, it seems appropriate to inquire about *quantitative* advancement, in terms of performance criteria, *for the specific tasks considered*, retinal vessel segmentation and classification. For this purpose we attempted a quantitative analysis of the performance of the non-DL and DL methods surveyed. This, in turn, is far from straightforward.

The largest sample of methods that can be evaluated as homogeneously as possible was achieved considering methods tested on DRIVE and STARE only, with accuracy as the only reference criterion. In the time period considered in this survey, this led to a sample of 17 DL and 33 non-DL papers for DRIVE, and 13 DL and 25 non-DL papers for STARE. This represents a total of 88 paper out of the 158 included in the survey: homogeneity is achieved at the expenses of inclusivity.

We computed normalized histogram plots of the average accuracy on DRIVE and STARE (Fig. 3), the normalized histogram was computed by dividing the number of observations in each bin with total number of observations. Separate accuracies for healthy and diseased images are reported in various papers (Table A.1 to Table A.3); we used the accuracy for healthy images in our analysis.

The resulting histograms are shown in Fig. 3a) for STARE Fig. 3b) for DRIVE.

For STARE, the answer to our questions is *yes*: most DL methods surveyed achieve clearly better accuracy than most non-DL ones,

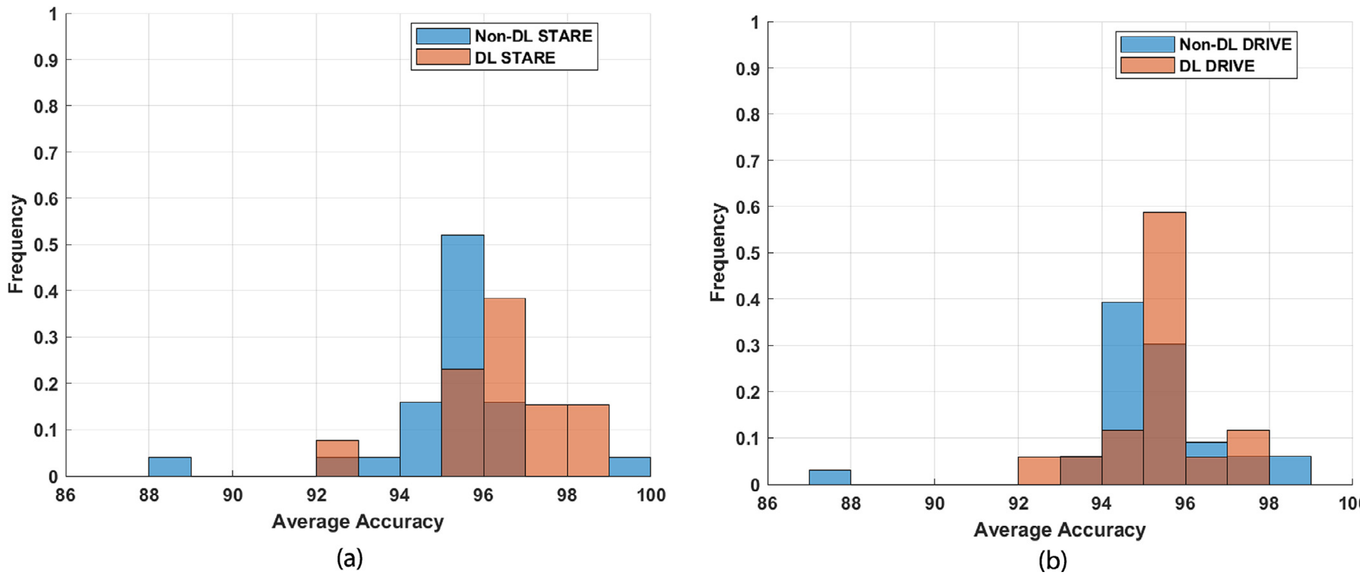

Fig. 3. Normalized histogram of average accuracy for (a) STARE database; (b) DRIVE database.

and the overall best accuracy is better for DL methods (~99% vs. ~96%). For DRIVE, however, the answer is not so clear. Unlike the STARE case, the DL and non-DL histograms are hardly separable. The majority of DL and non-DL methods reach their best accuracy, respectively, at around 95 and 96% and around 94 and 95%, arguably rather close; the overall best accuracy is attained by non-DL methods, although again close to the best DL one (~99% vs ~98%).

Within the limits of our analysis, discussed in the next paragraph, we are tempted to conclude that DL has not yet made a clear, significant improvement of accuracy *for the specific problem* of retinal vessel detection with DRIVE and STARE.

This conclusion cannot but be suggestive, given the many limiting factors.

First, as mentioned, different papers use different datasets and criteria, making it hard to compare algorithms fairly.

Second, and consequently, the sample analysed is smaller than the total number of papers to guarantee fair comparison (17 DL and 33 non-DL papers for DRIVE, and 13 DL and 25 non-DL papers for STARE).

Third, even using the same datasets and criteria, test protocols may differ (e.g. number of folds, proportions of data for training vs. testing).

Fourth, DRIVE and STARE have resolutions of, respectively, 584×565 and 700×605, considerably smaller than that of state-of-the-art fundus cameras. But then, is our analysis useful at all? We think so, for two main reasons. (a) As our review shows, DRIVE is the benchmark data set encountered most frequently in the retinal image processing papers reviewed, and new papers keep including it in their tests. There is a need for public, *annotated* data sets of images at contemporary resolution (around 3000×3000). Some such data sets are beginning to emerge, e.g. in international challenges like MICCAI REFUGE, or HRF, but they are still nowhere as widely used in the literature as DRIVE. (b) Several algorithms, especially high-accuracy DL ones, begin by downscaling the raw images to DRIVE-like size, typically to limit processing times. The advantage of a higher instrument resolution is therefore substantially reduced or lost altogether. This is arguably only temporary: increasingly powerful, accessible and affordable computing platforms will eventually overcome this limitation, and the increase in computing power are unlikely to be paralleled by the increase in image size (fundus image resolutions are already close to the maximum resolution allowed by the optical system of fundus cameras).

Fifth, it would be wrong to conclude that DL is not making a difference for retinal image analysis *in general*. We have focused on two very specific image processing tasks, vessel segmentation and classification; DL has generated breakthrough work on retinal biomarkers, suggesting for instance that the retina alone can predict, sometimes with unexpected accuracy, personal attributes and disease presence (De Fauw et al., 2018). This is the domain of contemporary artificial intelligence classification, of which image processing may or may not be a component.

Finally, we have concentrated on fundus camera images; image analysis systems exist for images from further instruments like SLO, OCT, optical coherence tomography angiography (OCT-A) and autofluorescence, which provide insights into different parts and processes of the retina (Mookiah et al., 2015).

7.3. Performance and specific challenges

We listed in Section 2.2 a number of recognized challenges specific to the tasks of vessel segmentation and classification with retinal fundus camera images:

1. central light reflex, splitting a single vessel in two parallel ones;
2. poorly contrasted small vessels, missed in the vessel map;
3. broken vessels at bifurcations/crossover points;
4. close, parallel vessels segmented as a single large one, merging two vessels into a single one;
5. imaging artefacts, e.g. noise, non-uniform illumination, blur, creating false positives and/or false negatives;
6. lesions like microaneurysm, exudates, cotton wool spots and haemorrhages, creating false positives or interrupting vessels.

The evaluation criteria used normally (accuracy, precision, recall, AUC) suggest only indirectly how well an algorithm meets the challenges above. We suggest therefore that challenge-specific criteria should be also used, for instance the ones below (item numbers correspond to the list above).

1. The amount of vessels broken by central reflection, requiring annotations of the vessels to check. These should be easily obtained as central reflections tend to occur on major vessels only.
2. The amount of small-vessel pixels missed by the algorithm, e.g. comparing histograms of true positives and false negatives over width bins for ground truth and algorithm. This could be done over the whole image and/or in peripherals zones, i.e. far from

the optic disc. It would also be possible to collect annotations of "small vessels" for a given clinical task, as the definition is "small" may depend on the task.

3. The amount of junctions and bifurcations correctly identified (already used in various papers) and a comparison of widths near junctions and bifurcations, i.e., as usual, results against ground truth. "Near" could be defined as the radius of a circle centered on the estimated intersection points of the three vessels involved.
4. Same as the previous point, but we expect the volume of annotations required per image to be smaller as central reflection occurs more frequently than close, parallel vessels.
5. Images could be attributed scores (by annotators) reflecting the amount of artefacts they present, roughly proportional to the difficulty of achieving good-quality results, hence divided into groups. Performance could then be evaluated consistently within separate groups. We note that this challenge is linked with the problem of quality assessment. The definition of quality, arguably, depends on the purpose for which it is assessed, whether clinical (e.g. identifying images unsuitable for expert inspection in reading centers) or computational (e.g. selecting images unsuitable for a given algorithm, i.e. unlikely to generate reliable results). A full discussion of this topic is well beyond the scope of our review.
6. With STARE, DRIVE and other datasets, it is common to report values of accuracy or related criteria separately for healthy and diseased retinas when using datasets including both. This is customary for datasets created for automated scoring of DR like MESSIDOR, DRIVE and CHASEDB1. Similarly to the case of junctions and bifurcations, one could generate accuracy figures for vessel segmentation and classification near lesions, requiring of course annotations of the lesion regions as well as a definition of "near".

These criteria would require an additional effort in terms of annotation, but we argue that this effort would be offset by the advantage of a much more informative evaluation of the usefulness of an algorithm for applicative purposes.

8. Conclusions

This paper has presented a review of retinal vessel segmentation and artery/vein classification methods published in the last six years, with an emphasis on machine and deep learning. Accurate segmentation and artery/vein classification is needed for the development of computer assisted systems for screening and diagnosis of retinal and microvascular diseases. Artery/vein classification is important for clinical diagnosis and clinical association studies, as the arteriolar and venular networks may exhibit different morphological parameters like vessel caliber measurements (e.g. central retinal artery equivalent (CRAE), central retinal vein equivalent (CRVE), and AVR), commonly adopted in the clinical literature of retinal biomarkers (e.g. cardiovascular disease (CVD) (Wong et al., 2001), hypertension (Wong et al., 2001), stroke (Doubal et al., 2009), dementia (McGrory et al., 2017) and cognitive impairment (Taylor et al., 2015)) and computed by semi-automated retinal vessel analysis tools such as vascular assessment and measurement platform for images of the retina (VAMPIRE) (Perez-Rovira et al., 2011a), SIVA (Lau et al., 2013), interative vessel analysis (IVAN) (Wong et al., 2004), and automated tools such as quantitative analysis of retinal vessel topology (QUARTZ) (Fraz et al., 2015), and ARIA (Bankhead et al., 2012).

The current panorama of public data sets suggests that the development of accurate methods for vessel detection and classification, especially with DL methods, requires much larger collection of images from state-of-the-art instruments, as many as possible annotated (Moccia et al., 2018). While the collection of large sets of images for research is now underway (see for instance UK Biobank, with about 50,000 retinal images linked to patient data), generating a large number of annotations remains an open problem. The recent experience at Moorfields, UK De Fauw et al. (2018) indicates a mismatch between the amount of images obtained (~1.5M) and what could be actually annotated by many experts (three orders of magnitude less). Research aimed to reduce the number of annotations needed seems particularly important to achieve all-round automation on a large scale (Valindria et al., 2017; Joyce et al., 2018; Huo et al., 2018; Kohlberger et al., 2012).

Asking clinicians to circle or highlight specific elements in retinal images forces them to do something they would not do normally. The consequence is additional time (hard to find) and risk of boredom hence errors. A way to reduce the need for expensive annotations in some cases is validation on outcome, i.e. testing the whole system of which a specific module is part (e.g. the performance of an automatic DR screening tool instead of the accuracy of the microaneurysm detector module).

Several tasks seem solved reasonably well by non-DL methods. Key here is the term "reasonably", which, in our view, should ultimately be defined in terms of the application (validation on outcome), not just of module-specific validation. In other words, the best vessel segmentation technique should be the one which improves the most the performance (as defined for the application) of a healthcare task (e.g. assisted diagnosis, patient triage, DR screening), at a parity of other factors; and not necessarily the one that achieves, say, the best AUC on specific, limited test set- especially if this means very small differences compared to other methods, which may or not be relevant for the target healthcare application. As the international debate on validation progresses, it will be extremely interesting to see what validation paradigms ultimately prevail.

To conclude, evaluating the effectiveness and merit of a technique should be done, ultimately, with respect to its contribution to the healthcare applications in which it is deployed, or at least *on outcome*, i.e. comparing the benefits, ceteris paribus, to the application using the results of vessel classification and segmentation methods, e.g. vessel-based biomarker discovery for predicting the risk of systemic diseases. This is a much larger task than we set out to accomplish.

Declaration of Competing Interest

I (we) certify that there is no conflict of interest with any financial organization regarding the material discussed in the paper.

CRediT authorship contribution statement

Muthu Rama Krishnan Mookiah: Conceptualization, Methodology, Investigation, Writing - original draft. **Stephen Hogg:** Investigation, Writing - review & editing. **Tom J MacGillivray:** Writing - review & editing. **Vijayaraghavan Prathiba:** Writing - review & editing. **Rajendra Pradeepa:** Writing - review & editing. **Viswanathan Mohan:** Supervision, Writing - review & editing, Funding acquisition. **Ranjit Mohan Anjana:** Supervision, Writing - review & editing. **Alexander S. Doney:** Writing - review & editing. **Colin N.A. Palmer:** Funding acquisition, Supervision, Writing - review & editing. **Emanuele Trucco:** Funding acquisition, Supervision, Conceptualization, Methodology, Writing - original draft, Writing - review & editing.

Acknowledgements

This research was funded by the National Institute for Health Research (NIHR) (INSPIRED 16/136/102) using UK aid from the

UK Government to support global health research. The views expressed in this publication are those of the author(s) and not necessarily those of the NIHR or the UK Department of Health and Social Care.

Appendix A

Table A.1-11

Table A1
Summary of vessel segmentation using deep learning.

Author (Year)	Method	Dataset (No. of images)	Se (%) *TPR	Sp (%) *FPR	Acc (%)	AUC *DICE
Maji et al. (2015)	***Preprocessing:*** NA ***Features:*** CNN feature representation ***Classifier:*** Random forest	DRIVE (40)	–	–	93.27	0.92
Wang et al. (2015)	***Preprocessing:*** Super pixel based sample selection using linear iterative clustering ***Features:*** Learned hierarchical features using CNN ***Classifier:*** Random forest	DRIVE (40) STARE (20)	81.73 81.04	97.33 97.91	97.67 98.13	– –
Fu et al. (2016b)	***Preprocessing:*** NA ***Features:*** CNN feature representation ***Classifier:*** CRF	DRIVE (40) STARE (20)	72.94 71.40	– –	94.70 95.45	– –
Fu et al. (2016a)	***Preprocessing:*** NA ***Features:*** CNN feature representation ***Classifier:*** CRF	DRIVE (40) STARE (20) CHASEDB1 (28)	76.03 74.12 71.30	– – –	95.23 95.85 94.89	– – –
Liskowski and Krawiec (2016)	***Preprocessing:*** Global contrast normalization, ZCA ***Features:*** CNN feature representation ***Classifier:*** Structured prediction	DRIVE (40) STARE (20) CHASEDB1 (28)	78.11 85.54 –	98.07 98.62 –	95.35 97.29 95.38	– – –
Luo et al. (2016)	***Preprocessing:*** NA ***Features:*** CNN feature representation using VGG-Net ***Classifier:*** CRF	DRIVE (40)	–	–	95.36	–
Maninis et al. (2016)	***Preprocessing:*** NA ***Features:*** CNN feature representation using GoogLeNet ***Classifier:*** Sigmoid	DRIVE (40) STARE (20)	– –	– –	– –	0.82 0.83
Dasgupta and Singh (2017)	***Preprocessing:*** CLAHE ***Features:*** FCN feature representation using U-Net ***Classifier:*** Softmax	DRIVE (40)	76.91	98.01	95.33	–
Meyer et al. (2017)	***Preprocessing:*** NA ***Features:*** FCN feature representation using U-Net ***Classifier:*** Sigmoid	IOSTAR (30) RC-SLO (40)	80.38 80.90	98.01 97.94	96.95 96.23	–
Mo and Zhang (2017)	***Preprocessing:*** NA ***Features:*** FCN feature representation ***Classifier:*** Sigmoid	DRIVE (40) STARE (20) CHASEDB1 (28)	77.79 81.47 76.61	97.80 98.44 98.16	95.21 96.74 95.99	– – –
Tan et al. (2017)	***Preprocessing:*** RGB to LUV color space ***Features:*** CNN feature representation ***Classifier:*** Softmax	DRIVE (40)	77.96	97.17	–	–
Zhou et al. (2017)	***Preprocessing:*** Luminosity and contrast normalization ***Features:*** Modified CNN model in MatCovnNet ***Classifier:*** Dense conditional random field	DRIVE (40) STARE (20) CHASEDB1 (28) HRF (45)	80.78 80.65 75.53 80.15	96.74 97.61 97.51 96.99	94.69 95.85 95.20 95.44	– – – –
Brancati et al. (2018)	***Preprocessing:*** NA ***Features:*** CNN and directional filter based feature representation ***Classifier:*** Sigmoid	DRIVE (40)	78.2	97.6	94.9	–
Guo et al. (2018)	***Preprocessing:*** NA ***Features:*** CNN based feature representation ***Classifier:*** Softmax	DRIVE (40) STARE (20)	–	–	91.99 92.20	–
Hu et al. (2018)	***Preprocessing:*** NA ***Features:*** CNN and CRF based feature representation ***Classifier:*** Sigmoid	DRIVE (40) STARE (20)	77.72 75.43	97.93 98.14	95.33 96.32	– –
Jiang et al. (2018)	***Preprocessing:*** CLAHE ***Features:*** FCN based feature representation using AlexNet ***Classifier:*** Softmax	DRIVE (40) STARE (30) CHASEDB1 (28) HRF (45)	75.40 83.52 86.40 80.10	98.25 98.46 97.45 80.10	96.24 97.34 96.68 96.50	– – – –
Oliveira et al. (2018)	***Preprocessing:*** NA ***Features:*** SWT and FCN based feature representation ***Classifier:*** Softmax	DRIVE (40) STARE (30) CHASEDB1 (28)	80.39 83.15 77.79	98.04 98.58 98.64	95.76 96.94 96.53	– – –
Xu et al. (2018)	***Preprocessing:*** Histogram matching ***Features:*** FCN based feature representation ***Classifier:*** Softmax	DRIVE (40) INSPIRE (40)	87 –	98 –	– –	– –
Yan et al. (2018b)	***Preprocessing:*** Data augmentation ***Features:*** FCN based feature representation ***Classifier:*** Sigmoid	DRIVE (40) STARE (20) CHASEDB1 (28)	76.31 77.35 76.41	98.20 98.57 98.06	95.38 96.38 96.07	– – –

(continued on next page)

Table A1 (*continued*)

Yan et al. (2018a)	***Preprocessing:*** NA ***Features:*** FCN based feature representation ***Classifier:*** Sigmoid	DRIVE (40) STARE (20) CHASEDB1 (28) HRF (45)	76.53 75.81 76.33 78.81	98.18 98.46 98.09 95.92	95.42 96.12 96.10 94.37	– – – –
Zhao et al. (2018a)	***Preprocessing:*** NA ***Features:*** GANs ***Classifier:*** Tanh	DRIVE (40) STARE (20) HRF (45)	80.38 78.96 80.01	98.15 98.41 98.23	– – –	– – –
Park et al. (2020)	***Preprocessing:*** Automatic color equalization ***Features:*** M-GANs ***Classifier:*** Softmax	DRIVE (40) STARE (20) CHASEDB1 (28) HRF (45)	83.46 83.24 – –	98.36 99.38 – –	97.06 98.76 97.36 97.61	0.99 0.99 0.99 0.99

Table A2
Summary of vessel segmentation using other machine learning methods.

Author (Year)	Method	Dataset (No. of images)	Se (%) *TPR	Sp (%) *FPR	Acc (%)	AUC *DICE
Cao et al. (2012)	***Preprocessing:*** NA ***Features:*** Steerable wavelet filter, Patch-based feature vector ***Classifier:*** NN	DRIVE (40)	–	–	–	0.98
Condurache and Mertins (2012)	***Preprocessing:*** Top hat and botton hat transform, Hessian single and multi-scale, Band-pass filter, and Laplacian pyramid ***Features:*** Multidimensional pixel feature space ***Classifier:*** Hysteresis relative LDA	DRIVE (40) STARE (20)	90.94 89.02	95.91 96.73	95.16 95.95	– –
Fraz et al. (2012c)	***Preprocessing:*** NA ***Features:*** 9-D feature vector (orientation analysis of the gradient vector field, morphological transformation, line strength measure, and Gabor filter response) ***Classifier:*** Ensemble classifier	DRIVE (40) STARE (20) CHASEDB1 (28)	74.06 75.48 72.24	98.07 97.63 97.11	94.80 95.34 94.69	0.98 0.98 0.97
Zhang et al. (2012)	***Preprocessing:*** NA ***Features:*** Multi-scale Matched Filter ***Classifier:*** Sparse representation classifier	DRIVE (40) STARE (20)	*58 *74	*0.28 *0.48	– –	– –
Fathi and Naghsh-Nilchi (2013b)	***Preprocessing:*** NA ***Features:*** Multi-scale rotation-invariant LBP ***Classifier:*** Adaptive neuro-fuzzy inference system	DRIVE (40) STARE (20)	*74 *76	*3.91 *4.35	94.18 94.14	– –
Cheng et al. (2014)	***Preprocessing:*** NA ***Features:*** Position related features, Orientation invariant features ***Classifier:*** Random forest classifier	DRIVE (40) STARE (20)	72.52 78.13	97.98 98.43	94.74 96.33	– –
Fathi and Naghsh-Nilchi (2014)	***Preprocessing:*** Top-hat transform, Length filtering ***Features:*** Position related features, Orientation invariant features ***Classifier:*** MLP-ANN	DRIVE (40)	76.49	3.75	94.49	–
Franklin and Rajan (2014)	***Preprocessing:*** Background normalization using arithmetic mean kernel, CLAHE ***Features:*** Color features ***Classifier:*** NN	DRIVE (40)	68.67	98.24	95.03	–
Fraz et al. (2014)	***Preprocessing:*** Dual Gaussian, Second derivative of Gaussian, Gabor filters ***Features:*** Multi-scale line strength measure ***Classifier:*** Ensemble classification	CHASEDB1 (28)	72.59	97.70	95.24	–
Ganjee et al. (2014)	***Preprocessing:*** AHE, MF-FDOG ***Features:*** Shape features ***Classifier:*** SVM-RBF	STARE (20)	*72	*1.91	95.36	–
Orlando and Blaschko (2014)	***Preprocessing:*** NA ***Features:*** Fully-connected conditional random field ***Classifier:*** Structured output SVM	DRIVE (40)	78.5	96.7	–	–
Rahebi and Hardalaç (2014)	***Preprocessing:*** Median filter ***Features:*** Co-occurrence matrix, Harlick features ***Classifier:*** NN	DRIVE (40) STARE (20)	73.65 69.02	97.07 98.04	94.61 95.27	– –
Sigurðsson et al. (2014)	***Preprocessing:*** CLAHE, Gaussian filter, Top-hat operator, Edge detection using Difference of Gaussian ***Features:*** Directional filtering ***Classifier:*** Fuzzy classifier	DRIVE (40)	–	–	94.55	–

(*continued on next page*)

Table A2 (*continued*)

Ding et al. (2015)	***Preprocessing:*** Vessel-Line filter, Hyteresis thresholding ***Features:*** Multi-fractal and Fourier fractal features ***Classifier:*** SVM-RBF	STARE (60) MESSIDOR (76)	– –	– –	92.8 79.6	– –
Zhang et al. (2015)	***Preprocessing:*** NA ***Features:*** Gabor filter, SIFT ***Classifier:*** *k*-means clustering, 1-NN	DRIVE (40)	78.12	96.68	95.05	–
Vega et al. (2015)	***Preprocessing:*** Gaussian kernel, Top-hat operator ***Features:*** Moment invariant pixel representation ***Classifier:*** Lattice NN	DRIVE (40) STARE (20)	74.44 70.19	96 96.71	94.12 94.83	– –
Waheed et al. (2015)	***Preprocessing:*** Multi-layered thresholding technique ***Features:*** Shape and intensity based features, Localized Fisher Discriminant Analysis ***Classifier:*** SVM	DRIVE (40) STARE (20) AFIO (462)	*84.02 *77.80 *86.20	*97.49 *97.45 *95.04	96.33 95.91 91.98	– – –
Annunziata and Trucco (2016)	***Preprocessing:*** NA ***Features:*** SCIRD-TS filter ***Classifier:*** Random decision forest	DRIVE (40) STARE (20)	–	–	–	0.87 0.86
Aslani and Sarnel (2016)	***Preprocessing:*** CLAHE ***Features:*** Gabor filter responses, B-COSFIRE filter, Eigen analysis of Hessian matrix ***Classifier:*** Radom forest classifier	DRIVE (40) STARE (20)	75.45 75.56	98.01 98.37	95.13 96.05	– –
GeethaRamani and Balasubramanian (2016)	***Preprocessing:*** Color space transformation, CLAHE ***Features:*** Gabor filtering, Halfwave rectification, PCA ***Classifier:*** Ensemble classification	DRIVE (40)	70.79	97.78	95.36	–
Li et al. (2016)	***Preprocessing:*** NA ***Features:*** Cross-modality learning ***Classifier:*** Wide and deep NN	DRIVE (40) STARE (20) CHASEDB1 (28)	75.69 77.26 75.07	98.16 98.44 97.93	95.27 96.28 95.81	– – –
Panda et al. (2016)	***Preprocessing:*** Highboost filtering, Arithmetic mean kernel ***Features:*** Edge distance seeded region growing, *k*-means clustering ***Classifier:*** SVM	DRIVE (40) STARE (20) HRF (45)	73.28 84.03 81.42	97.52 95.04 95.25	95.39 94.24 94.20	– – –
Strisciuglio et al. (2016)	***Preprocessing:*** B-COSFIRE filter, Difference-of-Gaussians ***Features:*** Generalized matrix learning vector quantization ***Classifier:*** SVM	DRIVE (40) STARE (20)	77.77 80.46	97.02 97.10	94.54 95.34	– –
Zhu et al. (2016)	***Preprocessing:*** Gaussian filter, Top hat and botton hat transform ***Features:*** Divergence of vector fields, CART ***Classifier:*** AdaBoost	DRIVE (40) RIS (10)	74.62 83.19	98.38 96.07	96.18 95.35	– –
Barkana et al. (2017)	***Preprocessing:*** AHE, Background correction using morphological operations ***Features:*** Pixel intensity statistics ***Classifier:*** Fuzzy system, ANN, SVM	DRIVE (40) STARE (20)	72.24 70.14	98.40 98.46	95.02 95.53	– –
Kalaie and Gooya (2017)	***Preprocessing:*** Green channel extraction ***Features:*** Intensity profile ***Classifier:*** PGM	REVIEW (16) DRIVE (89)	*88.6 *97	*99.1 *79.6	98.4 98.9	–
Kaur and Mittal (2017)	***Preprocessing:*** Unsharp masking, MF-FDOG ***Features:*** Shape and intensity features ***Classifier:*** NN	DRIVE (40) STARE (20) ARIA (212) HRF (45) Clinical (468)	87.23 83.0 88.51 87.51 87.67	98.69 97.30 98.92 98.2 96.96	94.80 95.91 94.87 94.34 94.82	– – – – –
Javidi et al. (2017)	***Preprocessing:*** AHE ***Features:*** FDDL ***Classifier:*** GMM	DRIVE (40) STARE (20)	72.01 77.80	97.02 96.53	94.50 95.17	– –
Memari et al. (2017)	***Preprocessing:*** CLAHE, B-COSFIRE, Frangi filter ***Features:*** Pixel statistics, texture, and Gabor-based features ***Classifier:*** AdaBoost	DRIVE (40) STARE (20) CHASEDB1 (28)	87.26 80.85 81.92	98.84 97.98 95.91	97.2 95.1 94.8	– – –
Orlando et al. (2017a)	***Preprocessing:*** Mathematical morphology ***Features:*** 2D Gabor wavelet, Multi-scale line detectors, Fully connected conditional random field ***Classifier:*** Structured output SVM	HRF (45)	76.69	97.25	–	–

(*continued on next page*)

Table A2 (*continued*)

Orlando et al. (2017b)	***Preprocessing:*** Mathematical morphology ***Features:*** Conditional random field model, Unary and pairwise features ***Classifier:*** Structured output SVM	DRIVE (40) STARE (20) CHASEDB1 (28) HRF (45)	78.97 76.80 72.77 78.74	96.84 97.28 97.12 95.84	– – – –	– – – –
Shah et al. (2017)	***Preprocessing:*** Median filter, CLAHE ***Features:*** Regional statistical features, Hessian features ***Classifier:*** Linear minimum squared error classifier	DRIVE (40)	*72.05	*1.9	94.79	–
Tang et al. (2017)	***Preprocessing:*** Median filter, CLAHE ***Features:*** Hessian feature, Influence degree of average intensity ***Classifier:*** SVM	DRIVE (40) STARE (20)	81.74 77.68	97.47 97.51	96.11 95.47	– –
Srinidhi et al. (2018)	***Preprocessing:*** CLAHE, Non-uniform sampling on polar grid, Visual attention modelling ***Features:*** *k*-means filter learning, ZCA whitening ***Classifier:*** Random forest classifier	DRIVE (40) STARE (20) CHASEDB1 (28) IOSTAR (30) RC-SLO (40)	86.44 83.25 82.97 82.69 84.88	96.67 97.46 96.63 96.69 96.66	95.89 95.02 94.74 95.64 95.81	0.97 0.97 0.96 0.97 0.97
Jebaseeli et al. (2019)	***Preprocessing:*** CLAHE ***Features:*** Tandem Pulse Coupled Neural Network feature representation ***Classifier:*** Deep Learning Based Support Vector Machine	DRIVE (40) STARE (20) REVIEW (16) HRF (45) DRIONS (110)	80.27 80.60 80.88 80.77 80.54	99.80 99.70 98.76 99.66 99.78	98.98 99.70 99.87 98.96 99.94	– – – – –

Table A3
Summary of vessel segmentation using unsupervised methods.

Author (Year)	Method	Dataset (No. of images)	Se (%) *TPR	Sp (%) *FPR	Acc (%)	AUC *DICE
Dai et al. (2015)	***Preprocessing:*** NA ***Features:*** Gray-voting, 2D Gabor filter ***Classifier:*** GMM	DRIVE (40) STARE (20)	73.59 77.69	97.20 95.50	94.18 93.64	– –
Hassanien et al. (2015)	***Preprocessing:*** Brightness correction ***Features:*** Artificial bee colony optimization ***Classifier:*** FCM	DRIVE (40) STARE (20)	72.1 64.9	97.1 98.2	93.88 94.68	–
Roychowdhury et al. (2015a)	***Preprocessing:*** High pass filter ***Features:*** Pixel-based classification ***Classifier:*** GMM	DRIVE (40) STARE (20)	72.5 77.2	98.3 97.3	95.2 95.1	– –
Oliveira et al. (2016)	***Preprocessing:*** Contrast stretching, Matched filter, Frangis filter ***Features:*** Gabor wavelet filter ***Classifier:*** FCM	DRIVE (40) STARE (20)	*86.44 *82.54	*4.44 *3.53	94.64 95.32	0.95 0.95
Emary et al. (2017)	***Preprocessing:*** Brightness correction ***Features:*** Flower pollination search algorithm, Pattern search algorithm, *k*-means ***Classifier:*** FCM, PFCM	DRIVE (40)	–	–	93.68	–
Neto et al. (2017)	***Preprocessing:*** Gaussian smoothing, Top-hat operator ***Features:*** Spatial dependency and probability computation ***Classifier:*** Global statistical thresholding	DRIVE (40) STARE (20)	78.06 83.44	96.29 94.43	87.18 88.94	– –
Hassan and Hassanien (2018)	***Preprocessing:*** Multi-level thresholding ***Features:*** Bee colony swarm optimization ***Classifier:*** FCM	DRIVE (40)	89.81	98.83	97.93	–

Table A4
Summary of vessel segmentation using matched filtering.

Author (Year)	Method	Dataset (No. of images)	Se (%) *TPR	Sp (%) *FPR	Acc (%)	AUC *DICE
Ramlugun et al. (2012)	***Preprocessing:*** CLAHE ***Filtering Method:*** 2D Matched filters ***Thresholding:*** Hysteresis thresholding	DRIVE (40)	64.13	97.67	93.1	–
Odstrcilik et al. (2013)	***Preprocessing:*** Morphological operators ***Filtering Method:*** Two-dimensional matched filters ***Thresholding:*** Kittler minimum error thresholding method	DRIVE (40) STARE (20) HRF (45)	70.60 78.47 78.61	96.93 95.12 97.50	93.40 93.41 95.39	0.95 0.93 0.95
Koukounis et al. (2014)	***Preprocessing:*** Gaussian low pass filtering ***Filtering Method:*** Matched filter ***Thresholding:*** Iterative thresholding	DRIVE (40) STARE (20)	– –	– –	92.4 –	0.90 –
Kar and Maity (2016b)	***Preprocessing:*** Curvelet-based edge enhancement ***Filtering Method:*** Matched filter, Laplacian of Gaussian filter ***Thresholding:*** Area thresholding	DRIVE (40)	*76.33	*1.91	96.54	0.97% (DRIVE)
Kar and Maity (2016a)	***Preprocessing:*** CLAHE, Curvelet transform ***Filtering Method:*** Matched filtering, Laplacian of Gaussian filter ***Thresholding:*** Area thresholding	DRIVE (40) STARE (20) DIARETDB1 (89)	75.48 75.77 –	97.92 97.88 –	96.16 97.30 –	– – –
Kar and Maity (2016c)	***Preprocessing:*** Curvelet transform ***Filtering Method:*** Matched filtering using 2D kernel ***Thresholding:*** Fuzzy conditional entropy	DRIVE (40) STARE (20) DIARETDB1 (89)	*76.32 *75.61	*1.9 *2.1	96.28 97.06	– –
Kovács and Hajdu (2016)	***Preprocessing:*** CLAHE ***Filtering Method:*** Gabor filter, Template matching and contour reconstruction ***Thresholding:*** Thresholding	DRIVE (40) STARE (20) HRF (45)	74.50 80.34 75.25	97.93 97.86 98.90	94.94 96.10 96.78	0.97 0.98 –
Krause et al. (2016)	***Preprocessing:*** Radon transform ***Filtering Method:*** Gaussian kernel ***Thresholding:*** Thresholding ***Postprocessing:*** Prairie-fire algorithm	DRIVE (40)	*75.17	*2.59	94.68	–
Tan et al. (2016)	***Preprocessing:*** Background correction and uneven illumination ***Filtering Method:*** Medial filter, Gabor filtering ***Thresholding:*** Thresholding ***Postprocessing:*** Thinning, Ramer–Douglas–Peucker algorithm	DRIVE (40)	–	–	93.18	–
Liu et al. (2016)	***Preprocessing:*** NA ***Filtering Method:*** B-COSFIRE filters, Multiscale centreline-boundary contrast map, Diffusion map ***Classifier:*** SVM	DRIVE (40) STARE (20)	77.18 78.22	97.07 97.45	94.51 95.41	– –
Singh and Srivastava (2016)	***Preprocessing:*** CLAHE, PCA, Gumbel probability distribution function ***Filtering Method:*** Matched filter ***Thresholding:*** Entropy based optimal thresholding ***Postprocessing:*** Length filtering	DRIVE (40) STARE (20)	*75.94 *79.39	*2.92 *6.24	95.22 92.70	– –
Subudhi et al. (2016)	***Preprocessing:*** Median filter ***Filtering Method:*** MF-FDOG ***Thresholding:*** Thresholding ***Postprocessing:*** Particle swarm optimization	DRIVE (40)	34.5	97.2	91.1	–
Farokhian et al. (2017)	***Preprocessing:*** Green channel extraction ***Filtering Method:*** Gabor filtering ***Thresholding:*** Thresholding	DRIVE (40)	69.33	97.77	93.92	0.95
Rezaee et al. (2017)	***Preprocessing:*** Wiener filter, Brightness correction ***Filtering Method:*** Matched Filter ***Thresholding:*** Fuzzy entropy-based thresholding	DRIVE (40) STARE (20)	71.89 72.02	97.93 97.41	94.63 95.21	– –
Soomro et al. (2017)	***Preprocessing:*** Uneven illumination correction using morphological closing, PCA ***Filtering Method:*** 2D Gaussian filter, Anisotropic oriented diffusion filter ***Thresholding:*** Hysteresis thresholding	DRIVE (40) STARE (20)	75.23 78.4	97.6 98.1	94.32 96.14	0.97 0.98

Table A5
Summary of vessel segmentation using morphological image processing.

Author (Year)	Method	Dataset (No. of images)	Se (%) *TPR	Sp (%) *FPR	Acc (%)	AUC *DICE
Fraz et al. (2012a)	***Preprocessing:*** Large arithmetic mean kernel, Maximum principal curvature ***Morphological processing:*** FoDoG filter, Bit planes slicing ***Thresholding:*** NA	DRIVE (40) STARE (20) MESSIDOR (1200)	71.52 73.11 75.02	97.59 96.80 97.85	94.30 94.42 95.7	– –
Saleh and Eswaran (2012)	***Preprocessing:*** AHE ***Morphological processing:*** Top-hat and bottom-hat transform, H-maxima transformation ***Thresholding:*** Multi-level thresholding	DRIVE (40)	*84.31	*2.83	96.53	–
Badsha et al. (2013)	***Preprocessing:*** Kirschs template, AHE ***Morphological processing:*** closing, erosion ***Thresholding:*** NA	DRIVE (40)	98.99	86	97.31	–
Fraz et al. (2013)	***Preprocessing:*** NA ***Morphological processing:*** Top-hat transform, Bit planes slicing, Oriented difference of offset Gaussian filter ***Postprocessing:*** Region growing	DRIVE (40) STARE (20)	73.02 73.18	97.42 96.60	94.22 94.23	– –
Imani et al. (2015)	***Preprocessing:*** NA ***Morphological processing:*** Morphological component analysis, Morlet Wavelet Transform ***Thresholding:*** Adaptive thresholding	DRIVE (40) STARE (20)	75.24 75.02	97.53 97.45	95.23 95.90	– –
Dash and Bhoi (2017)	***Preprocessing:*** CLAHE, Median filter ***Morphological processing:*** Morphological operations ***Thresholding:*** *C*-means thresholding	DRIVE (40) CHASEDB1 (28)	*71.9 *70.4	*97.6 *97.6	95.5 95.4	– –
Hassan et al. (2017)	***Preprocessing:*** NA ***Morphological processing:*** Mean kernel, Hidden Markov model ***Thresholding:*** Adaptive thresholding, Otsu thresholding	DRIVE (40)	80.5	96.56	95.7	0.90
Jiang et al. (2017)	***Preprocessing:*** NA ***Morphological processing:*** Top-hat transform, Difference of offset Gaussians filters ***Thresholding:*** Intensity thresholding, Adaptive thresholding	DRIVE (40) STARE (20)	83.75 77.67	96.94 97.05	95.97 95.79	– –

Table A6
Summary of vessel segmentation using vessel tracing and tracking methods.

Author (Year)	Method	Dataset (No. of images)	Se (%) *TPR	Sp (%) *FPR	Acc (%)	AUC *DICE
Lin et al. (2012)	***Preprocessing:*** NA ***Features:*** Likelihood ratio vesselness, Eigenvalue of multi-scale Hessian, Matched filter response, Tensor voting, Kalman filter ***Tracing/Tracking Method:*** Minimum-cost matching algorithm	DRIVE (40) FA database (6)	– –	– –	88.79 90.09	– –
Nayebifar and Moghad-dam (2013)	***Preprocessing:*** Median filter ***Features:*** Particle filter response ***Tracing/Tracking Method:*** Hysteresis thresholding	DRIVE (40) STARE (20)	*77.46 *72.78	*2.09 *1.26	– –	– –
Wang et al. (2013a)	***Preprocessing:*** NA ***Features:*** Vesselness computation, Matched filter response, Non-maximum suppression ***Tracing/Tracking Method:*** RBF kernel regression	DRIVE (40) RetCam (15) NIDEK (15)	– – –	– – –	82.3 80.6 81.2	– – –
Bekkers et al. (2014)	***Preprocessing:*** NA ***Features:*** NA ***Tracing/Tracking Method:*** ETOS, CTOS	HRIS VDIS CLRIS KPIS (16)	– – – –	– – – –	100 100 99.87 99.83	– – – –
Zhang et al. (2014)	***Preprocessing:*** NA ***Features:*** MAP estimation using Bayesian theory ***Tracing/Tracking Method:*** Multi-scale line detection	HRIS VDIS CLRIS KPIS (16)	– – – –	– – – –	100 98.3 94.2 100	– – – –
Nergiz and Akın (2017)	***Preprocessing:*** CLAHE, Frangi filter ***Features:*** 4D tensor field, Energy, anisotropy and orientation feature ***Tracing/Tracking Method:*** Otsu thresholding and tensor coloring	DRIVE (40) STARE (20) CHASEDB1 (28)	81.23 81.26 72.46	93.42 94.42 94.53	91.83 93.12 92.36	0.87 0.88 0.84
Yang et al. (2017)	***Preprocessing:*** Shape-weighed contrast enhancement ***Features:*** Vesselness filtering ***Tracing/Tracking Method:*** Pixel classification based on double thresholding	DRIVE (40)	–	–	–	*0.94
Khan et al. (2018)	***Preprocessing:*** CLAHE ***Features:*** Morphological filters, High boost filtering, Frangi filter ***Tracing/Tracking Method:*** Hysteresis threshold	DRIVE (40) STARE (20) HRF (45)	73 79.02 74.52	97.93 96.45 95.84	95.8 95.13 95.23	– –

Table A7
Summary of vessel segmentation using multi-scale methods.

Author (Year)	Method	Dataset (No. of images)	Se (%) *TPR	Sp (%) *FPR	Acc (%)	AUC *DICE
Bankhead et al. (2012)	***Preprocessing:*** NA ***Multi-scale processing:*** Isotropic undecimated wavelet transform, Anisotropic Gaussian filter ***Thresholding:*** NA ***Postprocessing:*** Morphological thinning, Centreline refinement using spline fitting	DRIVE (40)	*70.27	*2.8	93.71	–
Dizdaro et al. (2012)	***Preprocessing:*** NA ***Multi-scale processing:*** Log-Gabor filter, Local gradient, Eigenvalue of Hessian matrix ***Thresholding:*** NA	DRIVE (40)	71.81	97.43	94.12	–
Lazar and Hajdu (2012)	***Preprocessing:*** NA ***Multi-scale processing:*** Gaussian filter ***Thresholding:*** Hysteresis thresholding	DRIVE (40)	76.5	96.7	–	0.93
Li et al. (2012)	***Preprocessing:*** NA ***Multi-scale processing:*** Multi-scale matched filters ***Thresholding:*** Double-thresholding	DRIVE (40) STARE (20)	*71.54 *71.91	*2.84 *3.13	93.43 94.07	– –
Moghimirad et al. (2012)	***Preprocessing:*** NA ***Multi-scale processing:*** Vessel medialness detection filter ***Thresholding:*** Thresholding ***Postprocessing:*** Morphological operators	DRIVE (40) STARE (20)	*77.61 *89.49	*2.75 *6.10	94.73 93.54	– –
Fathi and Naghsh-Nilchi (2013a)	***Preprocessing:*** Multi-scale vessel enhancement ***Multi-scale processing:*** Complex continuous wavelet transform ***Thresholding:*** Adaptive thresholding ***Postprocessing:*** Length filtering	DRIVE (40) STARE (20)	77.68 80.61	97.59 97.17	95.81 95.91	– –
Liao et al. (2013)	***Preprocessing:*** NA ***Multi-scale processing:*** Fast marching, Multi-scale vesselness filter ***Thresholding:*** NA	DRIVE (40)	–	–	99.13	–
Nguyen et al. (2013)	***Preprocessing:*** NA ***Multi-scale processing:*** Multi-scale line detectors ***Thresholding:*** NA	DRIVE (40) STARE (20)	– –	– –	94.07 93.24	– –
Wang et al. (2013b)	***Preprocessing:*** NA ***Multi-scale processing:*** Matched filters with multiwavelet kernels, Multiscale hierarchical decomposition ***Thresholding:*** Adaptive thresholding	DRIVE (40) STARE (20)	– –	– –	94.61 95.21	– –
Hannink et al. (2014)	***Preprocessing:*** NA ***Multi-scale processing:*** Gaussian derivatives in orientation scores, Scale-orientation scores, Multi-scale Frangi vesselness filtering on scale-orientation scores ***Thresholding:*** NA	HRF (45)	78.6	98.8	96.9	–
Pellegrini et al. (2014)	***Preprocessing:*** NA ***Multi-scale processing:*** Laplacian of Gaussian, Gaussian filter, Eigenvalue analysis of the Hessian matrix ***Thresholding:*** Hysteresis thresholding	UWFoV SLO (10)	*70.2	*1.1	96.5	0.97
Zhao et al. (2014)	***Preprocessing:*** CLAHE ***Multi-scale processing:*** 2D Gabor wavelet, Anisotropic diffusion filter ***Postprocessing:*** Level-set method, Region growing	DRIVE (40) STARE (20)	73.54 71.87	97.89 97.67	94.77 95.09	– –
Zhen et al. (2014)	***Preprocessing:*** NA ***Multi-scale processing:*** Multi-scale directional contrast quantification ***Postprocessing:*** Differential fusion	DRIVE (40) STARE (20) HRF (45)	– – –	– – –	99 97 98	– – –
Lázár and Hajdu (2015)	***Preprocessing:*** NA ***Multi-scale processing:*** Pixelwise directional processing, 1D multiscale symmetric matched filter, 1D grayscale bottom-hat transform ***Postprocessing:*** Region growing, kNN	DRIVE (40) STARE (20) HRF (45)	*76.46 *72.48 *77.36	*2.77 *2.49 *1.63	94.58 94.92 95.72	– – –
Meng et al. (2015)	***Preprocessing:*** NA ***Multi-scale processing:*** ICGF, MMSDG ***Thresholding:*** Global threshold ***Postprocessing:*** Elongating filters	DRIVE (40) STARE (20)	74.89 74.13	98.18 98.25	95.29 95.69	– –
Annunziata et al. (2016)	***Preprocessing:*** Exudate inpainting technique ***Multi-scale processing:*** Multiscale Hessian Eigenvalue Analysis ***Thresholding:*** Percentile-Based Thresholding	STARE (20) HRF (45)	71.28 71.28	98.36 98.36	95.62 95.81	– –
BahadarKhan et al. (2016)	***Preprocessing:*** CLAHE ***Multi-scale processing:*** Hessian matrix and eigenvalues ***Thresholding:*** Otsu thresholding	DRIVE (40) STARE (20)	74.62 75.81	98.01 96.27	96.08 94.59	– –
Christodoulidis et al. (2016)	***Preprocessing:*** Estimation of luminosity and contrast ***Multi-scale processing:*** Dual-tree complex wavelet transform, Multi-scale line detection ***Thresholding:*** Adaptive thresholding ***Postprocessing:*** Multi-scale tensor voting framework	Erlangen database (45)	85.06	95.82	94.79	–

(continued on next page)

Table A7 (*continued*)

Zhang et al. (2016)	***Preprocessing:*** Morphological top-hat transform ***Multi-scale processing:*** Multi-scale second-order Gaussian derivatives, Eigenvalue analysis of left-invariant Hessian matrix ***Thresholding:*** NA	DRIVE (40) STARE (20) CHASEDB1 (28)	77.43 77.91 75.62	97.25 97.58 96.75	94.76 95.54 94.57	0.96 0.98 0.96
Guo et al. (2017)	***Preprocessing:*** NA ***Multi-scale processing:*** Shearlet transform, Neutrosophic inderminacy filtering, Multi-scale filter ***Classifier:*** NN	DRIVE (40) STARE (20)	– –	– –	– –	0.95 0.95
Pandey et al. (2017)	***Preprocessing:*** NA ***Multi-scale processing:*** Log-Gabor wavelet, Local phase preserving denoising ***Thresholding:*** Maximum entropy thresholding	DRIVE (40) STARE (20) CHASEDB1 (28) HRF (45)	81.06 83.19 81.06 80.25	97.61 96.23 95.30 96.29	96.23 94.44 94.94 95.76	0.97 0.96 0.96 0.96
Rodrigues and Marengoni (2017)	***Preprocessing:*** NA ***Multi-scale processing:*** Hessian based multi-scale filter ***Thresholding:*** Hysteresis thresholding	DRIVE (40) HRF (10)	71.65 72.23	98.01 96.36	94.65 94.72	– –
Zhang et al. (2017)	***Preprocessing:*** NA ***Multi-scale processing:*** Multi-scale second-order Gaussian derivatives, Wavelet, Pixel, and Gaussian scale-space features ***Classifier:*** Random Forest	DRIVE (40) STARE (20) CHASEDB1 (28)	78.61 78.82 –	97.12 97.29 –	94.66 95.47 –	0.97 0.97 –
Soomro et al. (2018)	***Preprocessing:*** Black top-hat transform, Independent component analysis, PCA ***Multi-scale processing:*** Multi-Scale Laplacian of Gaussian detector, Anisotropic oriented diffusion filter ***Postprocessing:*** Region growing, Morphological image reconstruction	DRIVE (40) STARE (20)	75.2 78.6	97.6 98.2	95.3 96.7	– –

Table A8
Summary of vessel segmentation using other methods.

Author (Year)	Method	Dataset (No. of images)	Se (%) *TPR	Sp (%) *FPR	Acc (%)	AUC *DICE
Dizdaroğlu et al. (2014)	***Preprocessing:*** AHE, Modified phase map ***Segmentation approach:*** Structure-based level set segmentation ***Thresholding:*** Otsu thresholding	DRIVE (40) STARE (20) Private (34)	77.04 69.29 51.79	96.13 97.26 98.10	93.65 94.41 94.41	– – –
Salazar-Gonzalez et al. (2014)	***Preprocessing:*** AHE ***Segmentation approach:*** Graph cut, Markov random field	DRIVE (40) STARE (20) DIARETDB1 (89)	*75.12 *78.87	*3.16 *3.67	94.12 94.41	– –
Roychowdhury et al. (2015b)	***Preprocessing:*** NA ***Segmentation approach:*** Morphological top-hat transformation ***Thresholding:*** Global thresholding, Adaptive thresholding ***Postprocessing:*** Region growing	DRIVE (40) STARE (20) CHASEDB1 (28)	73.9 73.2 –	97.8 98.4 –	94.9 95.6 –	0.97 0.97 –
Zhao et al. (2015a)	***Preprocessing:*** Retinex-based inhomogeneity correction, Local phase-based vessel enhancement ***Segmentation approach:*** Graph cut-based active contour method	DRIVE (40) STARE (20) ARIA (212) VAMPIRE (4)	74.4 78.6 75.1 72.1	97.8 97.5 93 98.4	95.3 95.1 94 97.6	0.86 0.88 0.84 0.85
Zhao et al. (2015b)	***Preprocessing:*** Eigenvalue-based, Wavelet-based, and Local Phase-Based Filter ***Segmentation approach:*** Infinite active contour with hybrid region information ***Postprocessing:*** Lebesgue measure, Hausdorff measure	DRIVE (40) STARE (20) VAMPIRE (4)	74.2 78 72.9	98.2 97.8 98.5	95.4 95.6 97.7	0.86 0.87 0.86
Asl et al. (2017)	***Preprocessing:*** Gaussian process ***Segmentation approach:*** Radon transform, Kernelized covariance matrix	DRIVE (40) STARE (20) CHASEDB1 (28) HRF (45)	74.28 74.19 75.35 77.15	97.32 97.06 97.67 97.57	– – – –	– – – –
Zhao et al. (2017)	***Preprocessing:*** Retinex-based inhomogeneity correction ***Segmentation approach:*** Compactness-based saliency segmentation, Infinite perimeter active contour	DRIVE (40) STARE (20)	78.2 78.9	97.9 97.8	95.7 95.6	0.89 0.89
Xue et al. (2018)	***Preprocessing:*** NA ***Segmentation approach:*** Texture saliency, Color saliency, Region optimization ***Thresholding:*** Histogram thresholding	DRIVE (40)	79.67	98.61	94.65	–

Table A9
Summary of artery/vein classification methods.

Author (Year)	Method	Dataset (No. of images)	Se (%) *TPR	Sp (%) *FPR	Acc (%)	AUC *DICE
Deep Learning Methods						
Girard and Cheriet (2017)	***Preprocessing:*** NA ***Features:*** CNN feature representation, Likelihood score propagation ***Classifier:*** Softmax	DRIVE (20) MESSIDOR (100)	92.3 (Ve) 90.6 (Ve)	93.1 (Ve) 97.6 (Ve)	86 (AV) 96.6 (AV)	– –
Welikala et al. (2017)	***Preprocessing:*** Mean filtering, Linear intensity transformation ***Features:*** CNN feature representation ***Classifier:*** Softmax	UK Biobank (100) DRIVE (40)	86.07 (A), 87.67 (V) –	87.67 (A), 86.07 (V) –	86.97(A), 86.97 (V) 91.97(AV)	– –
Xu et al. (2018)	***Preprocessing:*** Histogram matching ***Features:*** FCN feature representation using U-Net ***Classifier:*** Softmax	DRIVE (40) INSPIRE (40)	– –	– –	83.2 (AV) –	– –
Girard et al. (2019)	***Preprocessing:*** Illumination correction, Median filtering ***Features:*** CNN feature representation ***Classifier:*** Softmax ***Postprocessing:*** Likelihood score propagation	DRIVE (40) MESSIDOR (100)	86.3 (AV) 95.3 (AV)	86.6 (AV) 90.4 (AV)	86.5 (AV) 92.4 (AV)	– –
Hemelings et al. (2019)	***Preprocessing:*** Local contrast enhancement, Gaussian filter ***Features:*** FCN feature representation using U-Net ***Classifier:*** Softmax	DRIVE (40) HRF (45)	– –	– –	97.28 (AV) 94.25 (AV)	– –
Ma et al. (2019)	***Preprocessing:*** Illumination correction ***Features:*** FCN feature representation using U-Net ***Classifier:*** Sigmoid	AV-DRIVE (40) INSPIRE-AVR (40) HRF (45)	93.4 (AV) 92.4 (AV) –	95.5 (AV) 91.3 (AV) –	94.5 (AV) 91.6 (AV) –	– – –
Yang et al. (2020)	***Preprocessing:*** AHE, Morphologic bottom-hat transformation ***Features:*** Topological Structure, Constrained GANs ***Classifier:*** Softmax	DRIVE (40) CVDG (3119)	90.7 (AV) 88.5 (AV)	92.6 (AV) 91.2 (AV)	93.9 (AV) 93.6 (AV)	– –
Other Machine Learning Methods						
Dashtbozorg et al. (2013)	***Preprocessing:*** Large arithmetic mean kernel, Difference of offset Gaussians filters, Top-hat transform ***Features:*** Intensity features ***Classifier:*** LDA	INSPIRE-AVR (40)	–	–	91.1 (Ve), 98(AV)	–
Mirsharif et al. (2013)	***Preprocessing:*** MSRCR, Gabor wavelet ***Features:*** Color and statistical features of pixel intensity ***Classifier:*** LDA	DRIVE (40) Private (13)	– –	– –	82.65 (A), 85.74 (V), 84.05 (AV) 71.18 (A), 88.13 (V), 80.10 (AV)	– –
Dashtbozorg et al. (2014)	***Preprocessing:*** Large arithmetic mean kernel, Gaussian filters, Multiscale morphological vessel enhancement and reconstruction ***Features:*** Pixel intensity features ***Classifier:*** LDA, QDA, kNN	DRIVE (40) INSPIRE-AVR (40) VICAVR (20)	– – –	– – –	87.4 (AV) 88.3 (AV) 89.8 (AV)	– – –
Estrada et al. (2015a)	***Preprocessing:*** Graph-based topology estimation ***Features:*** Mean color value of RGB channel ***Classifier:*** Likelihood model, Heuristic search	WIDE (30) AV-DRIVE (40) CT-DRIVE (20) INSPIRE-AVR (40)	– – – –	– – – –	91 (AV) 93.5 (AV) 91.7 (AV) 90.9 (AV)	– – – –
Hu et al. (2015)	***Preprocessing:*** Graph analysis ***Features:*** Intensity-based features ***Classifier:*** SVM	RITE (40)	–	–	88.15 (AV)	–
Vijayakumar et al. (2016)	***Preprocessing:*** Median filte ***Features:*** GMM, Intensity-based and morphological features ***Classifier:*** Random forest, SVM	VICAVR (58)	90.87 (AV)	94.82 (AV)	92.4 (AV)	0.97 (AV)
Xu et al. (2017)	***Preprocessing:*** Gaussian filter ***Features:*** Gabor-based orientation features, vessel profile, color, and texture features ***Classifier:*** kNN	DRIVE (40)	–	–	91.5 (A) 92.9(V) 92.3(AV)	–
Yan et al. (2017)	***Preprocessing:*** CLAHE, Shifted filter response, B-COSFIRE, Different Gaussian filters ***Features:*** Morphology, topology and color features ***Classifier:*** JointBoost classifier	DRIVE (40)	–	–	94.5 (A) 91.1 (V)	–

(continued on next page)

Table A9 (*continued*)

Zhu et al. (2017)	***Preprocessing:*** Gaussian filter, Matched filter, Top hat and botton hat transform ***Features:*** Phase congruency, Hessian and divergence of vector fields ***Classifier:*** ELM	DRIVE (40)	71.40 (AV)	98.68 (AV)	96.07 (AV)	–
Zou et al. (2017)	***Preprocessing:*** Gaussian kernel ***Features:*** GLCM, Adaptive LBP ***Classifier:*** kNN	DRIVE (40) INSPIRE-AVR (40)	– –	– –	88.65 (AV) 88.51 (AV)	– –
Akbar et al. (2018)	***Preprocessing:*** CLAHE, 2D-GWT ***Features:*** Color and statistical features of pixel intensity ***Classifier:*** SVM-RBF	INSPIRE-AVR (40) VICAVR (58) Private (100)	94.25 (AV) 94.58 (AV) 98.34 (AV)	95.47 (AV) 95.83 (AV) 97.96 (AV)	95.10 (AV) 95.64 (AV) 98.09 (AV)	– – –
Huang et al. (2018)	***Preprocessing:*** Luminosity normalization using mean filter ***Features:*** Single-scale retinex, Color features ***Classifier:*** LDA	INSPIRE-AVR (40) NIDEK (45) VICAVR (58)	– – –	– – –	85.1 (AV) 86.9 (AV) 90.6(AV)	– – –
Pellegrini et al. (2018)	***Preprocessing:*** NA ***Features:*** NA ***Classifier:*** Linear Bayes classifier, Graph cut approach	WIDE (1) TASCFORCE (2)	– –	– –	86.4 (AV) 88.3 (AV)	– –
Srinidhi et al. (2019)	***Preprocessing:*** NA ***Features:*** Vessel keypoint descriptor, Graph representation, Line detector response, Histogram of oriented gradients ***Classifier:*** Random forest	AV-DRIVE (20) CT-DRIVE (20) INSPIRE-AVR (20) WIDE (15)	96.6 (AV) 95 (AV) 96.9 (AV) 92.3 (AV)	92.9 (AV) 91.5 (AV) 96.6 (AV) 88.2 (AV)	94.7 (AV) 93.2 (AV) 96.8 (AV) 90.2 (AV)	– – – –
Yin et al. (2020)	***Preprocessing:*** Background subtraction ***Features:*** Gabor Wavelet, Statistical measures of histogram, Different filter responses of images, and Local gradient information ***Classifier:*** kNN, SVM, Naive Bayes	INSPIRE-AVR (40) VICAVR (58) Private (44)	95.52 (AV) 85.08 (AV) 90.45 (AV)	92.34 (AV) 90.79 (AV) 90.45 (AV)	93.90 (AV) 87.82 (AV) 90.45 (AV)	– – –
Unsupervised Methods						
Relan et al. (2013)	***Preprocessing:*** NA ***Features:*** Color features ***Classifier:*** GMM-EM	Private (25)	–	–	92 (Ve) 85.47 (A) 87.19 (V)	–
Joshi et al. (2014)	***Preprocessing:*** Mosaicing, Gaussian filter ***Features:*** Dijkstra's graph search, Color features, Structural mapping ***Classifier:*** FCM	EYECHECK (50)	–	–	91.44 (AV)	–
Fu et al. (2017)	***Preprocessing:*** NA ***Features:*** Color features ***Classifier:*** *k*-means clustering	DRIVE (40)	–	–	93 (AV)	–
Relan et al. (2019)	***Preprocessing:*** Background correction, Median filtering ***Features:*** ROI-based, Profile-based, Contrast-based ***Classifier:*** GMM-EM	ORCADES (70) DRIVE (40)	– –	– –	86.7 (AV) 90.56 (AV)	– –
Zhao et al. (2019)	***Preprocessing:*** OD removal ***Features:*** Intensity, Orientation, Curvature, Diameter, and Entropy features ***Classifier:*** Topology estimation via dominant set clustering	INSPIRE (40) DRIVE (40) VICAVR (100) WIDE (30)	96.8 (AV) 94.2 (AV) 95.4 (AV) 96.2 (AV)	95.7 (AV) 92.7 (AV) 93.8 (AV) 94.2 (AV)	96.4 (AV) 93.5 (AV) 94.6 (AV) 95.2 (AV)	– – – –
Vessel Tracing and Tracking Methods						
Vázquez et al. (2013)	***Preprocessing:*** Retinex enhancement ***Features:*** Fast marching ***Tracing/Tracking Method:*** Minimal path approach	VICAVR (100)	–	–	87.68 (AV)	–
Lau et al. (2013)	***Preprocessing:*** NA ***Features:*** NA ***Tracing/Tracking Method:*** Graph tracer, Constraint optimization	Singapore Malay eye study database (2446)	98.9 (AV)	98.7 (AV)	–	–
Multi-scale Methods						
Eppenhof et al. (2015)	***Preprocessing:*** NA ***Multi-scale processing:*** Edge tracking in orientation scores, MRF, Local and Contextual features ***Classifier:*** Quadratic pseudo-boolean optimization algorithm	Private (150)	–	–	88 (Ve) 94 (AV)	–
Other Methods						
Remeseiro et al. (2020)	***Preprocessing:*** OD segmentation ***Segmentation approach:*** Local contrast, Graph computation ***Thresholding:*** Multilevel thresholding	DRIVE (40) INSPIRE (40)	88 (AV) 91 (AV)	79 (AV) 79 (AV)	– –	– –

Table A10
Segmentation challenges addressed by recent methods.

Author (Year)	OL	CVR	SM	BC	PV	IA
Deep Learning Methods						
Maji et al. (2015)	–	–	Yes	–	–	–
Fu et al. (2016b)	Yes	–	–	–	–	–
Fu et al. (2016a)	Yes	–	–	–	–	–
Liskowski and Krawiec (2016)	Yes	Yes	Yes	Yes	Yes	Yes
Luo et al. (2016)	Yes	–	–	–	–	–
Maninis et al. (2016)	–	–	Yes	–	–	–
Meyer et al. (2017)	–	–	–	–	–	Yes
Mo and Zhang (2017)	Yes	–	–	–	–	–
Zhou et al. (2017)	–	–	Yes	–	–	–
Xu et al. (2018)	Yes	–	Yes	–	–	–
Jiang et al. (2018)	Yes	–	Yes	–	–	–
Oliveira et al. (2018)	Yes	–	Yes	–	–	–
Yan et al. (2018b)	Yes	–	Yes	–	–	–
Yan et al. (2018a)	Yes	–	Yes	–	–	–
Park et al. (2020)	–	–	Yes	–	–	–
Other Machine Learning Methods						
Cao et al. (2012)	Yes	–	–	–	–	–
Condurache and Mertins (2012)	Yes	–	–	–	–	–
Fraz et al. (2012c)	Yes	–	–	–	–	–
Zhang et al. (2012)	Yes	–	Yes	–	–	–
Fathi and Naghsh-Nilchi (2013b)	–	–	Yes	–	–	–
Cheng et al. (2014)	Yes	–	–	–	–	–
Fathi and Naghsh-Nilchi (2014)	–	–	Yes	–	–	–
Fraz et al. (2014)	–	Yes	–	–	–	–
Ganjee et al. (2014)	Yes	–	–	–	–	–
Orlando and Blaschko (2014)	Yes	–	–	–	–	–
Sigurðsson et al. (2014)	–	–	Yes	–	–	–
Ding et al. (2015)	Yes	–	–	–	–	–
Zhang et al. (2015)	–	–	Yes	–	–	–
Vega et al. (2015)	Yes	–	Yes	–	–	–
Waheed et al. (2015)	Yes	–	–	–	–	–
Annunziata and Trucco (2016)	–	–	Yes	–	–	–
Aslani and Sarnel (2016)	Yes	–	–	–	–	–
Li et al. (2016)	Yes	Yes	Yes	Yes	Yes	Yes
Panda et al. (2016)	Yes	–	–	–	–	–
Strisciuglio et al. (2016)	–	–	Yes	–	–	–
Zhu et al. (2016)	Yes	–	–	–	–	–
Barkana et al. (2017)	Yes	–	–	–	–	–
Kalaie and Gooya (2017)	–	–	–	Yes	–	–
Kaur and Mittal (2017)	Yes	–	–	–	–	–
Javidi et al. (2017)	Yes	–	–	–	–	–
Memari et al. (2017)	Yes	–	Yes	–	–	–
Orlando et al. (2017a)	–	–	Yes	–	–	–
Orlando et al. (2017b)	Yes	–	–	–	–	–
Shah et al. (2017)	Yes	Yes	–	–	–	–
Tang et al. (2017)	Yes	–	–	–	–	–
Srinidhi et al. (2018)	Yes	Yes	Yes	Yes	Yes	Yes
Jebaseeli et al. (2019)	Yes	–	–	–	–	–
Unsupervised Methods						
Dai et al. (2015)	–	–	Yes	–	–	–
Hassanien et al. (2015)	Yes	–	Yes	–	–	–
Roychowdhury et al. (2015a)	Yes	–	–	–	–	–
Oliveira et al. (2016)	–	–	Yes	–	–	–
Emary et al. (2017)	Yes	–	–	–	–	–
Neto et al. (2017)	Yes	–	–	–	–	–
Hassan and Hassanien (2018)	Yes	–	–	–	–	–
Zhao et al. (2019)	–	–	–	Yes	–	–
Matched Filtering Methods						
Odstrcilik et al. (2013)	Yes	–	–	–	–	–
Kar and Maity (2016b)	Yes	–	–	–	–	Yes
Kar and Maity (2016a)	Yes	–	Yes	–	–	Yes
Kar and Maity (2016c)	Yes	–	Yes	–	–	Yes
Kovács and Hajdu (2016)	Yes	–	–	–	–	–
Krause et al. (2016)	–	–	–	Yes	–	–
Tan et al. (2016)	Yes	–	–	–	–	–
Rezaee et al. (2017)	Yes	–	Yes	–	–	–
Soomro et al. (2017)	Yes	–	–	–	–	–
Morphological Image Processing Methods						
Fraz et al. (2012a)	Yes	–	Yes	–	–	–
Fraz et al. (2013)	–	–	Yes	–	–	–
Imani et al. (2015)	Yes	–	–	–	–	–
Hassan et al. (2017)	–	–	Yes	–	–	–

(continued on next page)

Table A10 (*continued*)

Vessel Tracing and Tracking Methods						
Lin et al. (2012)	Yes	–	–	Yes	–	–
Nayebifar and Moghaddam (2013)	–	–	–	Yes	–	–
Wang et al. (2013a)	–	–	–	–	–	Yes
Bekkers et al. (2014)	–	–	–	Yes	Yes	–
Zhang et al. (2014)	–	–	–	Yes	–	–
Nergiz and Akın (2017)	Yes	–	–	–	–	–
Yang et al. (2017)	–	–	–	–	–	Yes
Khan et al. (2018)	Yes	–	Yes	–	–	–
Multi-scale Methods						
Bankhead et al. (2012)	–	Yes	–	–	–	–
Li et al. (2012)	–	–	Yes	–	–	–
Moghimirad et al. (2012)	Yes	–	Yes	–	–	–
Fathi and Naghsh-Nilchi (2013a)	Yes	–	–	–	–	–
Liao et al. (2013)	–	–	–	Yes	–	–
Nguyen et al. (2013)	–	Yes	–	–	Yes	–
Relan et al. (2013)	Yes	–	–	–	–	–
Wang et al. (2013b)	Yes	–	–	–	–	–
Hannink et al. (2014)	–	–	–	Yes	–	–
Joshi et al. (2014)	Yes	–	–	–	–	–
Zhao et al. (2014)	–	–	Yes	–	–	–
Zhen et al. (2014)	–	Yes	–	–	–	–
Lázár and Hajdu (2015)	Yes	–	–	–	–	–
Meng et al. (2015)	–	–	–	–	Yes	–
Annunziata et al. (2016)	Yes	–	–	–	–	–
BahadarKhan et al. (2016)	Yes	–	–	–	–	Yes
Christodoulidis et al. (2016)	Yes	Yes	–	–	–	–
Zhang et al. (2016)	–	Yes	Yes	–	Yes	–
Pandey et al. (2017)	Yes	–	Yes	–	–	–
Rodrigues and Marengoni (2017)	–	–	Yes	–	–	–
Zhang et al. (2017)	Yes	–	–	–	–	–
Other Methods						
Dizdaroğlu et al. (2014)	Yes	–	–	–	–	–
Roychowdhury et al. (2015b)	Yes	Yes	–	–	–	–
Zhao et al. (2015a)	–	–	–	–	Yes	Yes
Zhao et al. (2015b)	–	–	–	–	–	Yes
Asl et al. (2017)	–	Yes	Yes	–	–	–
Zhao et al. (2017)	Yes	Yes	–	–	–	–
Xue et al. (2018)	–	–	Yes	–	–	–
Artery/Vein Classification Methods						
Lau et al. (2013)	–	–	–	Yes	–	Yes
Mirsharif et al. (2013)	–	–	–	Yes	–	–
Vázquez et al. (2013)	–	–	–	Yes	–	–
Dashtbozorg et al. (2014)	–	–	–	Yes	–	–
Eppenhof et al. (2015)	–	–	–	Yes	–	–
Estrada et al. (2015a)	–	–	Yes	–	–	–
Hu et al. (2015)	–	–	Yes	–	–	–
Vijayakumar et al. (2016)	–	–	–	Yes	–	–
Fu et al. (2017)	–	–	–	–	–	Yes
Girard and Cheriet (2017)	Yes	–	Yes	–	–	–
Welikala et al. (2017)	–	–	–	Yes	Yes	–
Xu et al. (2017)	Yes	–	–	–	–	–
Yan et al. (2017)	–	–	Yes	–	–	–
Zhu et al. (2017)	Yes	–	–	–	–	–
Akbar et al. (2018)	Yes	–	–	–	–	–
Huang et al. (2018)	–	–	–	–	–	Yes
Pellegrini et al. (2018)	–	–	–	Yes	–	–
Girard et al. (2019)	Yes	–	Yes	–	–	–
Hemelings et al. (2019)	–	–	Yes	–	–	–
Ma et al. (2019)	–	–	–	–	Yes	–
Srinidhi et al. (2019)	–	–	–	Yes	–	–
Remeseiro et al. (2020)	–	–	–	Yes	–	–
Yang et al. (2020)	Yes	–	–	–	–	–
Yin et al. (2020)	Yes	–	–	–	–	–

Table A11
Summary of public databases for retinal vessel segmentation and artery/vein classification.

Dataset	Year	Image size	FOV	Image description			Annotations
				Fundus	FA	SLO	
Vessel Segmentation							
STARE Hoover et al. (2000)	2000	700 × 605	35°	Healthy (10) Pathology (10)	–	–	Two clinical experts
DRIVE Staal et al. (2004)	2004	584 × 565	45°	Training (20) Testing (20)	–	–	Two clinical experts
MESSIDOR Decenci'ere et al. (2014)	2004	1440 × 960 2240 × 1488 2304 × 1536	45°	Healthy (540) Pathology (660)	–	–	Not available
ARIA Zheng et al. (2012)	2006	768 × 576	50°	Healthy (61) DR (59) AMD (23)	–	–	Two clinical experts
DIARETDB1 Kälviäinen and Uusitalo (2007)	2007	1500 × 1152	50°	Healthy (05) DR (84)	–	–	Not available
REVIEW Al-Diri et al. (2008)	2008	3584 × 2438 1360 × 1024 2160 × 1440 288 × 119 170 × 92	–	HRIS (04) VDIS (08) CLRIS (02) KPIS (02)	–	–	Vessel widths marked by three human observers
CHASEDB1 Owen et al. (2009)	2011	1280 × 960	30°	Training (08) Testing (20)	–	–	Two clinical experts
HRF Budai et al. (2013)	2011	3504 × 2336	60°	Healthy (15) DR (15) Glaucoma (15)	–	–	One clinical expert
VAMPIRE Perez-Rovira et al. (2011b)	2011	3900 × 3072	200°	–	Healthy (04) AMD (04)	–	Three clinical experts
IOSTAR Zhang et al. (2016)	2015	1024 × 1024	45°	–	–	Healthy (30)	Group of clinical experts
RC-SLO Zhang et al. (2016)	2015	360 × 320	–	–	–	Healthy patches (40)	Group of clinical experts
Artery/Vein Classification							
INSPIRE-AVR Niemeijer et al. (2011)	2011	2392 × 2048	30°	Glaucoma (40)	–	–	Two clinical experts
VICAVR Vázquez et al. (2013)	2013	768 × 576	–	Healthy (100)	–	–	Two clinical experts
WIDE Estrada et al. (2015b)	2015	3900 × 3072	200°	Healthy (15) AMD (15)	–	–	Two clinical experts

List of acronyms in Table A1 to Table A11. MF-FDOG: matched filter with first-order derivative of Gaussian, Se: sensitivity, Sp: specificity, TPR: true positive rate, FPR: false positive rate, Acc: accuracy, AUC: area under roc, DICE: Dice similarity coefficient, AMTR: automatic/manually tracked ratio, FMTR: false/manually tracked ratio, HRIS: high resolution image set, VDIS: vascular disease image set, CLRIS: central light reflex image set, KPIS: KICK point image set, GLCM: gray level co-occurrence matrix, CLAHE: contrast limited adaptive histogram equalization, GWT: Gabor wavelet transform, MSRCR: multi-scale retinex with color restoration, AHE: adaptive histogram equalization, MLP: multilayer perceptrons, ELM: extreme learning machine, PPV: positive predictive value, FDDL: fisher discrimination dictionary learning, AUPRC: area under precision recall curves, QDA: quadratic discriminant analysis, PFCM: possibilistic fuzzy c-means, OL: obscuring lesions, SM: small vessels, BC: bifurcations/crossover points, PV: parallel vessels, IA: imaging artefacts, ICFG: improved circular Gabor filter, ZCA: zero-phase component analysis, IDM: inverse difference moment, PCA: principal component analysis, MAP: mean average precision, ETOS: edge tracking based on orientation scores, CTOS: centreline tracking based on multi-scale orientation scores, CART: classification and regression tree, PGM: probabilistic graphical model.

Supplementary material

Supplementary material associated with this article can be found, in the online version, at doi:10.1016/j.media.2020.101905.

References

Abràmoff, M.D., Garvin, M.K., Sonka, M., 2010. Retinal imaging and image analysis. IEEE Rev. Biomed. Eng. 3, 169–208.

Akbar, S., Akram, M.U., Sharif, M., Tariq, A., ullah Yasin, U., 2018. Arteriovenous ratio and papilledema based hybrid decision support system for detection and grading of hypertensive retinopathy. Comput. Methods Programs Biomed. 154, 123–141.

Al-Diri, B., Hunter, A., Steel, D., Habib, M., Hudaib, T., Berry, S., 2008. A reference data set for retinal vessel profiles. In: 2008 30th Annual International Conference of the IEEE Engineering in Medicine and Biology Society. IEEE, pp. 2262–2265.

Annunziata, R., Garzelli, A., Ballerini, L., Mecocci, A., Trucco, E., 2016. Leveraging multiscale hessian-based enhancement with a novel exudate inpainting technique for retinal vessel segmentation. IEEE J. Biomed. Health Inform. 20 (4), 1129–1138.

Annunziata, R., Trucco, E., 2016. Accelerating convolutional sparse coding for curvilinear structures segmentation by refining scird-ts filter banks. IEEE Trans. Med. Imaging 35 (11), 2381–2392.

Asl, M.E., Koohbanani, N.A., Frangi, A.F., Gooya, A., 2017. Tracking and diameter estimation of retinal vessels using gaussian process and radon transform. J. Med. Imaging 4 (3), 034006.

Aslani, S., Sarnel, H., 2016. A new supervised retinal vessel segmentation method based on robust hybrid features. Biomed. Signal Process. Control 30, 1–12.

Badsha, S., Reza, A.W., Tan, K.G., Dimyati, K., 2013. A new blood vessel extraction technique using edge enhancement and object classification. J. Digit. Imaging 26 (6), 1107–1115.

BahadarKhan, K., Khaliq, A.A., Shahid, M., 2016. A morphological hessian based approach for retinal blood vessels segmentation and denoising using region based otsu thresholding. PLoS ONE 11 (7), e0158996.

Bankhead, P., Scholfield, C.N., McGeown, J.G., Curtis, T.M., 2012. Fast retinal vessel detection and measurement using wavelets and edge location refinement. PLoS ONE 7 (3), e32435.

Barkana, B.D., Saricicek, I., Yildirim, B., 2017. Performance analysis of descriptive statistical features in retinal vessel segmentation via fuzzy logic, ann, svm, and classifier fusion. Knowl. Based Syst. 118, 165–176.

Bekkers, E., Duits, R., Berendschot, T., ter Haar Romeny, B., 2014. A multi-orientation analysis approach to retinal vessel tracking. J. Math. Imaging Vis. 49 (3), 583–610.

Brancati, N., Frucci, M., Gragnaniello, D., Riccio, D., 2018. Retinal Vessels Segmentation Based on a Convolutional Neural Network. In: Progress in Pattern Recognition, Image Analysis, Computer Vision, and Applications. Springer International Publishing, pp. 119–126. doi:10.1007/978-3-319-75193-1_15.

Budai, A., Bock, R., Maier, A., Hornegger, J., Michelson, G., 2013. Robust vessel segmentation in fundus images. Int. J. Biomed. Imaging 2013.
Bühler, K., Felkel, P., La Cruz, A., 2004. Geometric Methods for Vessel Visualization and Quantification a Survey. In: Geometric modeling for scientific visualization. Springer, pp. 399–419.
Cao, S., Bharath, A.A., Parker, K.H., Ng, J., 2012. Patch-based automatic retinal vessel segmentation in global and local structural context. In: Engineering in Medicine and Biology Society (EMBC), 2012 Annual International Conference of the IEEE. IEEE, pp. 4942–4945.
Chaudhuri, S., Chatterjee, S., Katz, N., Nelson, M., Goldbaum, M., 1989. Detection of blood vessels in retinal images using two-dimensional matched filters. IEEE Trans. Med. Imaging 8 (3), 263–269.
Cheng, E., Du, L., Wu, Y., Zhu, Y.J., Megalooikonomou, V., Ling, H., 2014. Discriminative vessel segmentation in retinal images by fusing context-aware hybrid features. Mach. Vis. Appl. 25 (7), 1779–1792.
Cheung, C.S., Butty, Z., Tehrani, N.N., Lam, W.C., 2011. Computer-assisted image analysis of temporal retinal vessel width and tortuosity in retinopathy of prematurity for the assessment of disease severity and treatment outcome. Journal of American Association for Pediatric Ophthalmology and Strabismus 15 (4), 374–380.
Christodoulidis, A., Hurtut, T., Tahar, H.B., Cheriet, F., 2016. A multi-scale tensor voting approach for small retinal vessel segmentation in high resolution fundus images. Computerized Medical Imaging and Graphics 52, 28–43.
Cinsdikici, M.G., Aydın, D., 2009. Detection of blood vessels in ophthalmoscope images using MF/ant (matched filter/ant colony) algorithm. Comput. Methods Programs Biomed. 96 (2), 85–95. doi:10.1016/j.cmpb.2009.04.005.
Condurache, A.P., Mertins, A., 2012. Segmentation of retinal vessels with a hysteresis binary-classification paradigm. Computerized Medical Imaging and Graphics 36 (4), 325–335.
Csincsik, L., Flynn, E., Pellegrini, E., Papanastasiou, G., MacGillivray, T., Ritchie, C.W., Peto, T., Lengyel, I., 2017. Assessing retinal vascular biomarkers for alzheimer's disease using ultra-widefield imaging (uwfi). Alzheimer's & Dementia: The Journal of the Alzheimer's Association 13 (7), P350.
Dai, P., Luo, H., Sheng, H., Zhao, Y., Li, L., Wu, J., Zhao, Y., Suzuki, K., 2015. A new approach to segment both main and peripheral retinal vessels based on gray-voting and gaussian mixture model. PLoS ONE 10 (6), e0127748.
Dasgupta, A., Singh, S., 2017. A fully convolutional neural network based structured prediction approach towards the retinal vessel segmentation. 2017 IEEE 14th International Symposium on Biomedical Imaging (ISBI 2017). IEEE doi:10.1109/isbi.2017.7950512.
Dash, J., Bhoi, N., 2017. A thresholding based technique to extract retinal blood vessels from fundus images. Future Computing and Informatics Journal 2 (2), 103–109. doi:10.1016/j.fcij.2017.10.001.
Dashtbozorg, B., Mendonça, A.M., Campilho, A., 2013. Automatic estimation of the arteriolar-to-venular ratio in retinal images using a graph-based approach for artery/vein classification. In: International Conference Image Analysis and Recognition. Springer, pp. 530–538.
Dashtbozorg, B., Mendonça, A.M., Campilho, A.J., 2014. An automatic graph-based approach for artery/vein classification in retinal images.. IEEE Trans. Image Processing 23 (3), 1073–1083.
De Fauw, J., Ledsam, J.R., Romera-Paredes, B., Nikolov, S., Tomasev, N., Blackwell, S., Askham, H., Glorot, X., O' Donoghue, B., Visentin, D., et al., 2018. Clinically applicable deep learning for diagnosis and referral in retinal disease. Nat. Med. 24 (9), 1342.
Deans, S.R., 2007. The radon transform and some of its applications. Courier Corporation.
Decenci'ere, E., Zhang, X., Cazuguel, G., Lay, B., Cochener, B., Trone, C., Gain, P., Ordonez, R., Massin, P., Erginay, A., Charton, B., Klein, J.-C., 2014. Feedback on a publicly distributed database: the messidor database. Image Analysis & Stereology 33 (3), 231–234. doi:10.5566/ias.1155.
Ding, Y., Ward, W., Duan, J., Auer, D., Gowland, P., Bai, L., 2015. Retinal vasculature classification using novel multifractal features. Physics in Medicine & Biology 60 (21), 8365.
Dizdaro, B., Ataer-Cansizoglu, E., Kalpathy-Cramer, J., Keck, K., Chiang, M.F., Erdogmus, D., 2012. Level sets for retinal vasculature segmentation using seeds from ridges and edges from phase maps. In: Machine Learning for Signal Processing (MLSP), 2012 IEEE International Workshop on. IEEE, pp. 1–6.
Dizdaroğlu, B., Ataer-Cansizoglu, E., Kalpathy-Cramer, J., Keck, K., Chiang, M.F., Erdogmus, D., 2014. Structure-based level set method for automatic retinal vasculature segmentation. EURASIP J. Image Video Process. 2014 (1), 39.
Doubal, F., Hokke, P., Wardlaw, J., 2008. Retinal microvascular abnormalities and stroke–a systematic review.. Journal of Neurology, Neurosurgery & Psychiatry.
Doubal, F., MacGillivray, T., Hokke, P., Dhillon, B., Dennis, M., Wardlaw, J., 2009. Differences in retinal vessels support a distinct vasculopathy causing lacunar stroke. Neurology 72 (20), 1773–1778.
Emary, E., Zawbaa, H.M., Hassanien, A.E., Parv, B., 2017. Multi-objective retinal vessel localization using flower pollination search algorithm with pattern search. Adv. Data Anal. Classif. 11 (3), 611–627.
Eppenhof, K., Bekkers, E., Berendschot, T.T., Pluim, J.P., ter Haar Romeny, B.M., 2015. Retinal artery/vein classification via graph cut optimization. In: Proceedings of the Ophthalmic Medical Image Analysis Second International Workshop. University of Iowa doi:10.17077/omia.1035.
Estrada, R., Allingham, M.J., Mettu, P.S., Cousins, S.W., Tomasi, C., Farsiu, S., 2015. Retinal artery-vein classification via topology estimation. IEEE Trans. Med. Imaging 34 (12), 2518–2534.
Estrada, R., Tomasi, C., Schmidler, S.C., Farsiu, S., 2015. Tree topology estimation. IEEE Trans Pattern Anal Mach Intell 37 (8), 1688–1701.
Farokhian, F., Yang, C., Demirel, H., Wu, S., Beheshti, I., 2017. Automatic parameters selection of gabor filters with the imperialism competitive algorithm with application to retinal vessel segmentation. Biocybernetics and Biomedical Engineering 37 (1), 246–254.
Fathi, A., Naghsh-Nilchi, A.R., 2013. Automatic wavelet-based retinal blood vessels segmentation and vessel diameter estimation. Biomed. Signal Process. Control 8 (1), 71–80.
Fathi, A., Naghsh-Nilchi, A.R., 2013. Integrating adaptive neuro-fuzzy inference system and local binary pattern operator for robust retinal blood vessels segmentation. Neural Computing and Applications 22 (1), 163–174.
Fathi, A., Naghsh-Nilchi, A.R., 2014. General rotation-invariant local binary patterns operator with application to blood vessel detection in retinal images. Pattern Analysis and Applications 17 (1), 69–81.
Faust, O., Acharya, R., Ng, E.Y.-K., Ng, K.-H., Suri, J.S., 2012. Algorithms for the automated detection of diabetic retinopathy using digital fundus images: a review. J. Med. Syst. 36 (1), 145–157.
Felkel, P., Wegenkittl, R., Kanitsar, A., 2001. Vessel tracking in peripheral cta datasets-an overview. In: Computer Graphics, Spring Conference on, 2001.. IEEE, pp. 232–239.
Franklin, S.W., Rajan, S.E., 2014. Computerized screening of diabetic retinopathy employing blood vessel segmentation in retinal images. biocybernetics and biomedical engineering 34 (2), 117–124.
Fraz, M.M., Barman, S.A., Remagnino, P., Hoppe, A., Basit, A., Uyyanonvara, B., Rudnicka, A.R., Owen, C.G., 2012. An approach to localize the retinal blood vessels using bit planes and centerline detection. Comput. Methods Programs Biomed. 108 (2), 600–616.
Fraz, M.M., Basit, A., Barman, S., 2013. Application of morphological bit planes in retinal blood vessel extraction. J. Digit. Imaging 26 (2), 274–286.
Fraz, M.M., Remagnino, P., Hoppe, A., Uyyanonvara, B., Rudnicka, A.R., Owen, C.G., Barman, S.A., 2012. Blood vessel segmentation methodologies in retinal images–a survey. Comput. Methods Programs Biomed. 108 (1), 407–433.
Fraz, M.M., Remagnino, P., Hoppe, A., Uyyanonvara, B., Rudnicka, A.R., Owen, C.G., Barman, S.A., 2012. An ensemble classification-based approach applied to retinal blood vessel segmentation. IEEE Trans. Biomed. Eng. 59 (9), 2538–2548.
Fraz, M.M., Rudnicka, A.R., Owen, C.G., Barman, S.A., 2014. Delineation of blood vessels in pediatric retinal images using decision trees-based ensemble classification. Int. J. Comput. Assist. Radiol. Surg. 9 (5), 795–811.
Fraz, M.M., Welikala, R., Rudnicka, A.R., Owen, C.G., Strachan, D., Barman, S.A., 2015. Quartz: quantitative analysis of retinal vessel topology and size–an automated system for quantification of retinal vessels morphology. Expert Syst. Appl. 42 (20), 7221–7234.
Fu, D., Liu, Y., Ma, H., 2017. An Artery/vein Classification Method Based on Color and Vascular Structure Information. In: Lecture Notes in Computer Science. Springer International Publishing, pp. 487–495. doi:10.1007/978-3-319-71589-6_42.
Fu, H., Xu, Y., Lin, S., Wong, D.W.K., Liu, J., 2016. DeepVessel: Retinal Vessel Segmentation Via deep Learning and Conditional Random field. In: Medical Image Computing and Computer-Assisted Intervention – MICCAI 2016. Springer International Publishing, pp. 132–139. doi:10.1007/978-3-319-46723-8_16.
Fu, H., Xu, Y., Wong, D.W.K., Liu, J., 2016. Retinal vessel segmentation via deep learning network and fully-connected conditional random fields. In: 2016 IEEE 13th international symposium on biomedical imaging (ISBI). IEEE, pp. 698–701.
Galdran, A., Costa, P., Bria, A., Araújo, T., Mendonça, A.M., Campilho, A., 2018. A no-reference quality metric for retinal vessel tree segmentation. In: International Conference on Medical Image Computing and Computer-Assisted Intervention. Springer, pp. 82–90.
Ganjee, R., Azmi, R., Gholizadeh, B., 2014. An improved retinal vessel segmentation method based on high level features for pathological images. J. Med. Syst. 38 (9), 108.
GeethaRamani, R., Balasubramanian, L., 2016. Retinal blood vessel segmentation employing image processing and data mining techniques for computerized retinal image analysis. Biocybernetics and Biomedical Engineering 36 (1), 102–118.
Girard, F., Cheriet, F., 2017. Artery/vein classification in fundus images using cnn and likelihood score propagation. In: 2017 IEEE Global Conference on Signal and Information Processing (GlobalSIP). IEEE, pp. 720–724.
Girard, F., Kavalec, C., Cheriet, F., 2019. Joint segmentation and classification of retinal arteries/veins from fundus images. Artif. Intell. Med. 94, 96–109.
Gonzalez, R.C., Woods, R.E., 2007. Image processing. Digital image processing 2, 1.
Guo, Y., Budak, Ü., Şengür, A., Smarandache, F., 2017. A retinal vessel detection approach based on shearlet transform and indeterminacy filtering on fundus images. Symmetry (Basel) 9 (10), 235.
Guo, Y., Budak, Ü., Vespa, L.J., Khorasani, E., Şengür, A., 2018. A retinal vessel detection approach using convolution neural network with reinforcement sample learning strategy. Measurement 125, 586–591.
Hannink, J., Duits, R., Bekkers, E., 2014. Crossing-preserving Multi-scale Vesselness. In: Medical Image Computing and Computer-Assisted Intervention – MICCAI 2014. Springer International Publishing, pp. 603–610. doi:10.1007/978-3-319-10470-6_75.
Haralick, R.M., Sternberg, S.R., Zhuang, X., 1987. Image analysis using mathematical morphology. IEEE Trans. Pattern Anal. Mach. Intell. (4) 532–550.
Hassan, G., Hassanien, A.E., 2018. Retinal fundus vasculature multilevel segmentation using whale optimization algorithm. Signal Image Video Process. 12 (2), 263–270 .

Hassan, M., Amin, M., Murtza, I., Khan, A., Chaudhry, A., 2017. Robust hidden markov model based intelligent blood vessel detection of fundus images. Comput. Methods Programs Biomed. 151, 193–201. doi:10.1016/j.cmpb.2017.08.023.

Hassanien, A.E., Emary, E., Zawbaa, H.M., 2015. Retinal blood vessel localization approach based on bee colony swarm optimization, fuzzy c-means and pattern search. J. Vis. Commun. Image Represent. 31, 186–196.

Hemelings, R., Elen, B., Stalmans, I., Van Keer, K., De Boever, P., Blaschko, M.B., 2019. Artery–vein segmentation in fundus images using a fully convolutional network. Computerized Medical Imaging and Graphics 76, 101636.

Hoover, A., Kouznetsova, V., Goldbaum, M., 2000. Locating blood vessels in retinal images by piecewise threshold probing of a matched filter response. IEEE Trans. Med. Imaging 19 (3), 203–210.

Hu, K., Zhang, Z., Niu, X., Zhang, Y., Cao, C., Xiao, F., Gao, X., 2018. Retinal vessel segmentation of color fundus images using multiscale convolutional neural network with an improved cross-entropy loss function. Neurocomputing 309, 179–191.

Hu, Q., Abràmoff, M.D., Garvin, M.K., 2015. Automated construction of arterial and venous trees in retinal images. J. Med. Imaging 2 (4), 044001.

Huang, F., Dashtbozorg, B., ter Haar Romeny, B.M., 2018. Artery/vein classification using reflection features in retina fundus images. Mach. Vis. Appl. 29 (1), 23–34.

Huo, Y., Xu, Z., Moon, H., Bao, S., Assad, A., Moyo, T.K., Savona, M.R., Abramson, R.G., Landman, B.A., 2018. Synseg-net: synthetic segmentation without target modality ground truth. IEEE Trans. Med. Imaging.

Imani, E., Javidi, M., Pourreza, H.-R., 2015. Improvement of retinal blood vessel detection using morphological component analysis. Comput. Methods Programs Biomed. 118 (3), 263–279.

Javidi, M., Pourreza, H.-R., Harati, A., 2017. Vessel segmentation and microaneurysm detection using discriminative dictionary learning and sparse representation. Comput. Methods Programs Biomed. 139, 93–108.

Jebaseeli, T.J., Durai, C.A.D., Peter, J.D., 2019. Retinal blood vessel segmentation from diabetic retinopathy images using tandem pcnn model and deep learning based svm. Optik (Stuttg) 199, 163328.

Jiang, Z., Yepez, J., An, S., Ko, S., 2017. Fast, accurate and robust retinal vessel segmentation system. Biocybernetics and Biomedical Engineering 37 (3), 412–421.

Jiang, Z., Zhang, H., Wang, Y., Ko, S.-B., 2018. Retinal blood vessel segmentation using fully convolutional network with transfer learning. Computerized Medical Imaging and Graphics 68, 1–15.

Joshi, V.S., Reinhardt, J.M., Garvin, M.K., Abramoff, M.D., 2014. Automated method for identification and artery-venous classification of vessel trees in retinal vessel networks. PLoS ONE 9 (2), e88061.

Joskowicz, L., Cohen, D., Caplan, N., Sosna, J., 2019. Inter-observer variability of manual contour delineation of structures in ct. Eur.. Radiol. 29 (3), 1391–1399.

Joyce, T., Chartsias, A., Tsaftaris, S.A., 2018. Deep multi-class segmentation without ground-truth labels.

Kalaie, S., Gooya, A., 2017. Vascular tree tracking and bifurcation points detection in retinal images using a hierarchical probabilistic model. Comput. Methods Programs Biomed. 151, 139–149.

Kälviäinen, R., Uusitalo, H., 2007. Diaretdb1 diabetic retinopathy database and evaluation protocol. In: Medical Image Understanding and Analysis, 2007. Citeseer, p. 61.

Kanski, J.J., Bowling, B., 2011. Clinical ophthalmology: A systematic approach. Elsevier Health Sciences.

Kar, S.S., Maity, S.P., 2016. Blood vessel extraction and optic disc removal using curvelet transform and kernel fuzzy c-means. Comput. Biol. Med. 70, 174–189.

Kar, S.S., Maity, S.P., 2016. Retinal blood vessel extraction and optic disc removal using curvelet transform and morphological operation. In: Singh, R., Vatsa, M., Majumdar, A., Kumar, A. (Eds.), Machine Intelligence and Signal Processing. Springer India, New Delhi, pp. 153–161.

Kar, S.S., Maity, S.P., 2016. Retinal blood vessel extraction using tunable bandpass filter and fuzzy conditional entropy. Comput. Methods Programs Biomed. 133, 111–132.

Kaur, J., Mittal, D., 2017. A generalized method for the detection of vascular structure in pathological retinal images. Biocybernetics and Biomedical Engineering 37 (1), 184–200.

Khan, K.B., Khaliq, A.A., Jalil, A., Shahid, M., 2018. A robust technique based on vlm and frangi filter for retinal vessel extraction and denoising. PLoS ONE 13 (2), e0192203.

Kirbas, C., Quek, F., 2004. A review of vessel extraction techniques and algorithms. ACM Computing Surveys (CSUR) 36 (2), 81–121.

Kohlberger, T., Singh, V., Alvino, C., Bahlmann, C., Grady, L., 2012. Evaluating segmentation error without ground truth. In: International Conference on Medical Image Computing and Computer-Assisted Intervention. Springer, pp. 528–536.

Köse, C., İki, C., et al., 2011. A personal identification system using retinal vasculature in retinal fundus images. Expert Syst. Appl. 38 (11), 13670–13681.

Koukounis, D., Ttofis, C., Papadopoulos, A., Theocharides, T., 2014. A high performance hardware architecture for portable, low-power retinal vessel segmentation. INTEGRATION, the VLSI journal 47 (3), 377–386.

Kovács, G., Hajdu, A., 2016. A self-calibrating approach for the segmentation of retinal vessels by template matching and contour reconstruction. Med. Image Anal. 29, 24–46.

Krause, M., Alles, R.M., Burgeth, B., Weickert, J., 2016. Fast retinal vessel analysis. Journal of Real-Time Image Processing 11 (2), 413–422.

Labate, D., Lim, W.-Q., Kutyniok, G., Weiss, G., 2005. Sparse multidimensional representation using shearlets. In: Wavelets XI, 5914. International Society for Optics and Photonics, p. 59140U.

Lau, Q.P., Lee, M.L., Hsu, W., Wong, T.Y., 2013. Simultaneously identifying all true vessels from segmented retinal images. IEEE Trans. Biomed. Eng. 60 (7), 1851–1858.

Lazar, I., Hajdu, A., 2012. Segmentation of vessels in retinal images based on directional height statistics. In: Engineering in Medicine and Biology Society (EMBC), 2012 Annual International Conference of the IEEE. IEEE, pp. 1458–1461.

Lázár, I., Hajdu, A., 2015. Segmentation of retinal vessels by means of directional response vector similarity and region growing. Comput. Biol. Med. 66, 209–221.

Li, H., Chutatape, O., 2004. Automated feature extraction in color retinal images by a model based approach. IEEE Trans. Biomed. Eng. 51 (2), 246–254.

Li, Q., Feng, B., Xie, L., Liang, P., Zhang, H., Wang, T., 2016. A cross-modality learning approach for vessel segmentation in retinal images.. IEEE Trans. Med. Imaging 35 (1), 109–118.

Li, Q., You, J., Zhang, D., 2012. Vessel segmentation and width estimation in retinal images using multiscale production of matched filter responses. Expert Syst. Appl. 39 (9), 7600–7610.

Li, T., Palmer, C., Pearson, E., MacGillivray, T., Trucco, E., Ballerini, L., Wang, R., Relan, D., Mckay, G., Doney, A., 2018. Retinal microvascular biomarkers are associated with incidence and progression of diabetic retinopathy in type 2 diabetes: A godarts-vampire study. DIABETIC MEDICINE, 35. WILEY 111 RIVER ST, HOBOKEN 07030-5774, NJ USA

Liao, W., Rohr, K., Wörz, S., 2013. Globally Optimal Curvature-regularized Fast Marching for Vessel Segmentation. In: Medical Image Computing and Computer-Assisted Intervention – MICCAI 2013. Springer Berlin Heidelberg, pp. 550–557. doi:10.1007/978-3-642-40811-3_69.

Lin, K.-S., Tsai, C.-L., Tsai, C.-H., Sofka, M., Chen, S.-J., Lin, W.-Y., 2012. Retinal vascular tree reconstruction with anatomical realism. IEEE Trans. Biomed. Eng. 59 (12), 3337–3347.

Lindeberg, T., 2013. Scale-space theory in computer vision, 256. Springer Science & Business Media.

Liskowski, P., Krawiec, K., 2016. Segmenting retinal blood vessels with _newline deep neural networks. IEEE Trans. Med. Imaging 35 (11), 2369–2380. doi:10.1109/tmi.2016.2546227.

Liu, Q., Zou, B., Chen, J., Chen, Z., Zhu, C., Yue, K., Zhao, G., 2016. Retinal vessel segmentation from simple to difficult. In: Proceedings of the Ophthalmic Medical Image Analysis Third International Workshop. University of Iowa doi:10.17077/omia.1047.

Luo, Y., Yang, L., Wang, L., Cheng, H., 2016. Efficient cnn-crf network for retinal image segmentation. In: International Conference on Cognitive Systems and Signal Processing. Springer, pp. 157–165.

Ma, W., Yu, S., Ma, K., Wang, J., Ding, X., Zheng, Y., 2019. Multi-task neural networks with spatial activation for retinal vessel segmentation and artery/vein classification. In: International Conference on Medical Image Computing and Computer-Assisted Intervention. Springer, pp. 769–778.

MacGillivray, T., Trucco, E., Cameron, J., Dhillon, B., Houston, J., Van Beek, E., 2014. Retinal imaging as a source of biomarkers for diagnosis, characterization and prognosis of chronic illness or long-term conditions. Br. J. Radiol. 87 (1040), 20130832.

Maier-Hein, L., Eisenmann, M., Reinke, A., Onogur, S., Stankovic, M., Scholz, P., Arbel, T., Bogunovic, H., Bradley, A.P., Carass, A., et al., 2018. Why rankings of biomedical image analysis competitions should be interpreted with care. Nat. Commun. 9 (1), 5217.

Maier-Hein, L., Eisenmann, M., Reinke, A., Onogur, S., Stankovic, M., Scholz, P., Arbel, T., Bogunovic, H., Bradley, A.P., Carass, A., et al., 2018. Why rankings of biomedical image analysis competitions should be interpreted with care. Nat. Commun. 9 (1), 1–13.

Maji, D., Santara, A., Ghosh, S., Sheet, D., Mitra, P., 2015. Deep neural network and random forest hybrid architecture for learning to detect retinal vessels in fundus images. In: 2015 37th annual international conference of the IEEE Engineering in Medicine and Biology Society (EMBC). IEEE, pp. 3029–3032.

Maninis, K.-K., Pont-Tuset, J., Arbeláez, P., Gool, L.V., 2016. Deep Retinal Image Understanding. In: Medical Image Computing and Computer-Assisted Intervention – MICCAI 2016. Springer International Publishing, pp. 140–148. doi:10.1007/978-3-319-46723-8_17.

McConnell, L.K., Nasser, O., Wahle, A., Lee, K., Abramoff, M.D., Kemp, P.S., 2017. Optical coherence tomography in pediatric optic nerve hypoplasia. Journal of American Association for Pediatric Ophthalmology and Strabismus {JAAPOS} 21 (4), e43.

McGrory, S., Cameron, J.R., Pellegrini, E., Warren, C., Doubal, F.N., Deary, I.J., Dhillon, B., Wardlaw, J.M., Trucco, E., MacGillivray, T.J., 2017. The application of retinal fundus camera imaging in dementia: a systematic review. Alzheimer's & Dementia: Diagnosis, Assessment & Disease Monitoring 6, 91–107.

McKay, G.J., Paterson, E.N., Maxwell, A.P., Cardwell, C.C., Wang, R., Hogg, S., MacGillivray, T.J., Trucco, E., Doney, A.S., 2018. Retinal microvascular parameters are not associated with reduced renal function in a study of individuals with type 2 diabetes. Sci. Rep. 8 (1), 3931.

Memari, N., Ramli, A.R., Saripan, M.I.B., Mashohor, S., Moghbel, M., 2017. Supervised retinal vessel segmentation from color fundus images based on matched filtering and adaboost classifier. PLoS ONE 12 (12), e0188939.

Meng, X., Yin, Y., Yang, G., Han, Z., Yan, X., 2015. A framework for retinal vasculature segmentation based on matched filters. Biomed. Eng. Online 14 (1), 94.

Meyer, M.I., Costa, P., Galdran, A., Mendonça, A., Campilho, A., 2017. A Deep Neural Network for Vessel Segmentation of Scanning Laser Ophthalmoscopy Images. In: Lecture Notes in Computer Science. Springer International Publishing, pp. 507–515. doi:10.1007/978-3-319-59876-5_56.

Mirsharif, Q., Tajeripour, F., Pourreza, H., 2013. Automated characterization of blood vessels as arteries and veins in retinal images. Computerized Medical Imaging and Graphics 37 (7–8), 607–617.
Mo, J., Zhang, L., 2017. Multi-level deep supervised networks for retinal vessel segmentation. Int. J. Comput. Assist. Radiol. Surg. 12 (12), 2181–2193. doi:10.1007/s11548-017-1619-0.
Moccia, S., De Momi, E., El Hadji, S., Mattos, L.S., 2018. Blood vessel segmentation algorithms-review of methods, datasets and evaluation metrics. Comput. Methods Programs Biomed. 158, 71–91.
Moghimirad, E., Rezatofighi, S.H., Soltanian-Zadeh, H., 2012. Retinal vessel segmentation using a multi-scale medialness function. Comput. Biol. Med. 42 (1), 50–60.
Mookiah, M.R.K., Acharya, U.R., Chua, C.K., Lim, C.M., Ng, E., Laude, A., 2013. Computer-aided diagnosis of diabetic retinopathy: areview. Comput. Biol. Med. 43 (12), 2136–2155.
Mookiah, M.R.K., Acharya, U.R., Fujita, H., Tan, J.H., Chua, C.K., Bhandary, S.V., Laude, A., Tong, L., 2015. Application of different imaging modalities for diagnosis of diabetic macular edema: a review. Comput. Biol. Med. 66, 295–315.
Nayebifar, B., Moghaddam, H.A., 2013. A novel method for retinal vessel tracking using particle filters. Comput. Biol. Med. 43 (5), 541–548.
Nergiz, M., Akın, M., 2017. Retinal vessel segmentation via structure tensor coloring and anisotropy enhancement. Symmetry (Basel) 9 (11), 276.
Neto, L.C., Ramalho, G.L., Neto, J.F.R., Veras, RM., Medeiros, F.N., 2017. An unsupervised coarse-to-fine algorithm for blood vessel segmentation in fundus images. Expert Syst. Appl. 78, 182–192.
Nguyen, U.T., Bhuiyan, A., Park, L.A., Ramamohanarao, K., 2013. An effective retinal blood vessel segmentation method using multi-scale line detection. Pattern Recognit. 46 (3), 703–715.
Niemeijer, M., Xu, X., Dumitrescu, A.V., Gupta, P., Van Ginneken, B., Folk, J.C., Abramoff, M.D., 2011. Automated measurement of the arteriolar-to-venular width ratio in digital color fundus photographs. IEEE Trans. Med. Imaging 30 (11), 1941–1950.
Odstrcilik, J., Kolar, R., Budai, A., Hornegger, J., Jan, J., Gazarek, J., Kubena, T., Cernosek, P., Svoboda, O., Angelopoulou, E., 2013. Retinal vessel segmentation by improved matched filtering: evaluation on a new high-resolution fundus image database. IET Image Proc. 7 (4), 373–383.
Oliveira, A., Pereira, S., Silva, C.A., 2018. Retinal vessel segmentation based on fully convolutional neural networks. Expert Syst. Appl. 112, 229–242.
Oliveira, W.S., Teixeira, J.V., Ren, T.I., Cavalcanti, G.D., Sijbers, J., 2016. Unsupervised retinal vessel segmentation using combined filters. PLoS ONE 11 (2), e0149943.
Orlando, J.I., Blaschko, M., 2014. Learning fully-connected crfs for blood vessel segmentation in retinal images. In: International Conference on Medical Image Computing and Computer-Assisted Intervention. Springer, pp. 634–641.
Orlando, J.I., Fracchia, M., del Río, V., del Fresno, M., 2017. Retinal blood vessel segmentation in high resolution fundus photographs using automated feature parameter estimation. SIPAIM.
Orlando, J.I., Fu, H., Bread, J.B., et al., 2019. Refuge challenge: a unified framework for evaluating automated methods for glaucoma assessment from fundus photographs. Med. Image Anal. 59. doi:10.1016/j.media.2019.101570.
Orlando, J.I., Prokofyeva, E., Blaschko, M.B., 2017. A discriminatively trained fully connected conditional random field model for blood vessel segmentation in fundus images. IEEE Trans. Biomed. Eng. 64 (1), 16–27.
Owen, C.G., Rudnicka, A.R., Mullen, R., Barman, S.A., Monekosso, D., Whincup, P.H., Ng, J., Paterson, C., 2009. Measuring retinal vessel tortuosity in 10-year-old children: validation of the computer-assisted image analysis of the retina (caiar) program. Investigative ophthalmology & visual science 50 (5), 2004–2010.
Panda, R., Puhan, N., Panda, G., 2016. New binary hausdorff symmetry measure based seeded region growing for retinal vessel segmentation. biocybernetics and biomedical engineering 36 (1), 119–129.
Pandey, D., Yin, X., Wang, H., Zhang, Y., 2017. Accurate vessel segmentation using maximum entropy incorporating line detection and phase-preserving denoising. Comput. Vision Image Understanding 155, 162–172.
Park, K.-B., Choi, S.H., Lee, J.Y., 2020. M-Gan: retinal blood vessel segmentation by balancing losses through stacked deep fully convolutional networks. IEEE Access.
Patton, N., Aslam, T.M., MacGillivray, T., Deary, I.J., Dhillon, B., Eikelboom, R.H., Yogesan, K., Constable, I.J., 2006. Retinal image analysis: concepts, applications and potential. Prog. Retin. Eye Res. 25 (1), 99–127.
Pellegrini, E., Robertson, G., MacGillivray, T., van Hemert, J., Houston, G., Trucco, E., 2018. A graph cut approach to artery/vein classification in ultra-widefield scanning laser ophthalmoscopy. IEEE Trans. Med. Imaging 37 (2), 516–526.
Pellegrini, E., Robertson, G., Trucco, E., MacGillivray, T.J., Lupascu, C., van Hemert, J., Williams, M.C., Newby, D.E., van Beek, E.J., Houston, G., 2014. Blood vessel segmentation and width estimation in ultra-wide field scanning laser ophthalmoscopy. Biomed. Opt. Express 5 (12), 4329–4337.
Perez-Rovira, A., MacGillivray, T., Trucco, E., Chin, K., Zutis, K., Lupascu, C., Tegolo, D., Giachetti, A., Wilson, P.J., Doney, A., et al., 2011. Vampire: vessel assessment and measurement platform for images of the retina. In: 2011 Annual International Conference of the IEEE Engineering in Medicine and Biology Society. IEEE, pp. 3391–3394.
Perez-Rovira, A., Zutis, K., Hubschman, J.P., Trucco, E., 2011. Improving vessel segmentation in ultra-wide field-of-view retinal fluorescein angiograms. In: 2011 Annual International Conference of the IEEE Engineering in Medicine and Biology Society. IEEE, pp. 2614–2617.
Rahebi, J., Hardalaç, F., 2014. Retinal blood vessel segmentation with neural network by using gray-level co-occurrence matrix-based features. J. Med. Syst. 38 (8), 85.
Ramlugun, G.S., Nagarajan, V.K., Chakraborty, C., 2012. Small retinal vessels extraction towards proliferative diabetic retinopathy screening. Expert Syst. Appl. 39 (1), 1141–1146.
Relan, D., Ballerini, L., Trucco, E., MacGillivray, T., 2019. Using orthogonal locality preserving projections to find dominant features for classifying retinal blood vessels. Multimed. Tools Appl. 78 (10), 12783–12803.
Relan, D., MacGillivray, T., Ballerini, L., Trucco, E., 2013. Retinal vessel classification: sorting arteries and veins. In: Engineering in Medicine and Biology Society (EMBC), 2013 35th Annual International Conference of the IEEE. IEEE, pp. 7396–7399.
Remeseiro, B., Mendonça, A.M., Campilho, A., 2020. Automatic classification of retinal blood vessels based on multilevel thresholding and graph propagation. Vis. Comput. 1–15.
Rezaee, K., Haddadnia, J., Tashk, A., 2017. Optimized clinical segmentation of retinal blood vessels by using combination of adaptive filtering, fuzzy entropy and skeletonization. Appl. Soft Comput. 52, 937–951.
Ricci, E., Perfetti, R., 2007. Retinal blood vessel segmentation using line operators and support vector classification. IEEE Trans. Med. Imaging 26 (10), 1357–1365.
Rodrigues, L.C., Marengoni, M., 2017. Segmentation of optic disc and blood vessels in retinal images using wavelets, mathematical morphology and hessian-based multi-scale filtering. Biomed. Signal Process. Control 36, 39–49.
Roychowdhury, S., Koozekanani, D.D., Parhi, K.K., 2015. Blood vessel segmentation of fundus images by major vessel extraction and subimage classification. IEEE J. Biomed. Health Inform. 19 (3), 1118–1128.
Roychowdhury, S., Koozekanani, D.D., Parhi, K.K., 2015. Iterative vessel segmentation of fundus images. IEEE Trans. Biomed. Eng. 62 (7), 1738–1749.
Salazar-Gonzalez, A.G., Kaba, D., Li, Y., Liu, X., 2014. Segmentation of the blood vessels and optic disk in retinal images.. IEEE J. Biomedical and Health Informatics 18 (6), 1874–1886.
Saleh, M.D., Eswaran, C., 2012. An efficient algorithm for retinal blood vessel segmentation using h-maxima transform and multilevel thresholding.. Comput. Methods Biomech. Biomed. Engin. 15 5. 517–25
Schapire, R.E., Singer, Y., 1999. Improved boosting algorithms using confidence-rated predictions. In: Machine Learning, pp. 80–91.
Serra, J., 1979. Biomedical image analysis by mathematical morphology (author's transl). Pathol. Biol. 27 (4), 205–207.
Shah, S.A.A., Tang, T.B., Faye, I., Laude, A., 2017. Blood vessel segmentation in color fundus images based on regional and hessian features. Graefe's Archive for Clinical and Experimental Ophthalmology 255, 1525–1533.
Sigurðsson, E.M., Valero, S., Benediktsson, J.A., Chanussot, J., Talbot, H., Stefánsson, E., 2014. Automatic retinal vessel extraction based on directional mathematical morphology and fuzzy classification. Pattern Recognit. Lett. 47, 164–171.
Silberzahn, R., Uhlmann, E.L., 2015. Crowdsourced research: many hands make tight work. Nature News 526 (7572), 189.
Singh, N.P., Srivastava, R., 2016. Retinal blood vessels segmentation by using gumbel probability distribution function based matched filter. Comput. Methods Programs Biomed. 129, 40–50.
Smith, W., Wang, J.J., Wong, T.Y., Rochtchina, E., Klein, R., Leeder, S.R., Mitchell, P., 2004. Retinal arteriolar narrowing is associated with 5-year incident severe hypertension: the blue mountains eye study. Hypertension 44 (4), 442–447.
Sofka, M., Stewart, C.V., 2006. Retinal vessel centerline extraction using multiscale matched filters, confidence and edge measures. IEEE Trans. Med. Imaging 25 (12), 1531–1546.
Sonka, M., Abràmoff, M.D., 2016. Quantitative analysis of retinal oct. Med. Image Anal. (33) 165–169.
Soomro, T.A., Khan, M.A.U., Gao, J., Khan, T.M., Paul, M., 2017. Contrast normalization steps for increased sensitivity of a retinal image segmentation method. Signal Image Video Process. 11, 1509–1517.
Soomro, T.A., Khan, T.M., Khan, M.A., Gao, J., Paul, M., Zheng, L., 2018. Impact of ica-based image enhancement technique on retinal blood vessels segmentation. IEEE Access 6, 3524–3538.
Srinidhi, C.L., Aparna, P., Rajan, J., 2017. Recent advancements in retinal vessel segmentation. J. Med. Syst. 41 (4), 70.
Srinidhi, C.L., Aparna, P., Rajan, J., 2018. A visual attention guided unsupervised feature learning for robust vessel delineation in retinal images. Biomed. Signal Process. Control 44, 110–126.
Srinidhi, C.L., Aparna, P., Rajan, J., 2019. Automated method for retinal artery/vein separation via graph search metaheuristic approach. IEEE Trans. Image Process. 28 (6), 2705–2718.
Staal, J., Abràmoff, M.D., Niemeijer, M., Viergever, M.A., Van Ginneken, B., 2004. Ridge-based vessel segmentation in color images of the retina. IEEE Trans. Med. Imaging 23 (4), 501–509.
Strisciuglio, N., Azzopardi, G., Vento, M., Petkov, N., 2016. Supervised vessel delineation in retinal fundus images with the automatic selection of b-cosfire filters. Mach. Vis. Appl. 27 (8), 1137–1149.
Subudhi, A., Pattnaik, S., Sabut, S., 2016. Blood vessel extraction of diabetic retinopathy using optimized enhanced images and matched filter. J. Med. Imaging 3 (4), 044003.
Sutter, F.K., Helbig, H., 2003. Familial retinal arteriolar tortuosity: a review. Surv. Ophthalmol. 48 (3), 245–255.
Tan, J.H., Acharya, U.R., Bhandary, S.V., Chua, K.C., Sivaprasad, S., 2017. Segmentation of optic disc, fovea and retinal vasculature using a single convolutional neural network. J. Comput. Sci. 20, 70–79.
Tan, J.H., Acharya, U.R., Chua, K.C., Cheng, C., Laude, A., 2016. Automated extraction of retinal vasculature. Med. Phys. 43 (5), 2311–2322.

Tang, Z., Zhang, J., Gui, W., 2017. Selective search and intensity context based retina vessel image segmentation. J. Med. Syst. 41 (3), 47.

Taylor, A.M., MacGillivray, T.J., Henderson, R.D., Ilzina, L., Dhillon, B., Starr, J.M., Deary, I.J., 2015. Retinal vascular fractal dimension, childhood iq, and cognitive ability in old age: the lothian birth cohort study 1936. PLoS ONE 10 (3), e0121119.

Teng, T., Lefley, M., Claremont, D., 2002. Progress towards automated diabetic ocular screening: a review of image analysis and intelligent systems for diabetic retinopathy. Med. Biol. Eng. Comput. 40 (1), 2–13.

Trucco, E., MacGillivray, T., (eds., Y.W., 2019. Computational retinal image analysis: Tools, applications and perspectives. Elsevier MICCAI Series.

Trucco, E., Ruggeri, A., Karnowski, T., Giancardo, L., Chaum, E., Hubschman, J.P., Al-Diri, B., Cheung, C.Y., Wong, D., Abramoff, M., et al., 2013. Validating retinal fundus image analysis algorithms: issues and a proposal. Investigative ophthalmology & visual science 54 (5), 3546–3559.

Valindria, V.V., Lavdas, I., Bai, W., Kamnitsas, K., Aboagye, E.O., Rockall, A.G., Rueckert, D., Glocker, B., 2017. Reverse classification accuracy: predicting segmentation performance in the absence of ground truth. IEEE Trans. Med. Imaging 36 (8), 1597–1606.

Vapnik, V., Guyon, I., Hastie, T., 1995. Support vector machines. Mach. Learn 20 (3), 273–297.

Vázquez, S., Cancela, B., Barreira, N., Penedo, M.G., Rodríguez-Blanco, M., Seijo, M.P., de Tuero, G.C., Barceló, M.A., Saez, M., 2013. Improving retinal artery and vein classification by means of a minimal path approach. Mach. Vis. Appl. 24 (5), 919–930.

Vega, R., Sanchez-Ante, G., Falcon-Morales, L.E., Sossa, H., Guevara, E., 2015. Retinal vessel extraction using lattice neural networks with dendritic processing. Comput. Biol. Med. 58, 20–30.

Vijayakumar, V., Koozekanani, D.D., White, R., Kohler, J., Roychowdhury, S., Parhi, K.K., 2016. Artery/vein classification of retinal blood vessels using feature selection. In: Engineering in Medicine and Biology Society (EMBC), 2016 IEEE 38th Annual International Conference of the. IEEE, pp. 1320–1323.

Vostatek, P., Claridge, E., Uusitalo, H., Hauta-Kasari, M., Fält, P., Lensu, L., 2017. Performance comparison of publicly available retinal blood vessel segmentation methods. Computerized Medical Imaging and Graphics 55, 2–12.

Waheed, A., Akram, M.U., Khalid, S., Waheed, Z., Khan, M.A., Shaukat, A., 2015. Hybrid features and mediods classification based robust segmentation of blood vessels. J. Med. Syst. 39 (10), 128.

Wang, L., Kallem, V., Bansal, M., Eledath, J., Sawhney, H., Karp, K., Pearson, D.J., Mills, M.D., Quinn, G.E., Stone, R.A., 2013. Interactive Retinal Vessel Extraction by Integrating Vessel Tracing and Graph Search. In: Medical Image Computing and Computer-Assisted Intervention – MICCAI 2013. Springer Berlin Heidelberg, pp. 567–574. doi:10.1007/978-3-642-40763-5_70.

Wang, S., Yin, Y., Cao, G., Wei, B., Zheng, Y., Yang, G., 2015. Hierarchical retinal blood vessel segmentation based on feature and ensemble learning. Neurocomputing 149, 708–717. doi:10.1016/j.neucom.2014.07.059.

Wang, Y., Ji, G., Lin, P., Trucco, E., 2013. Retinal vessel segmentation using multiwavelet kernels and multiscale hierarchical decomposition. Pattern Recognit. 46 (8), 2117–2133.

Webb, R.H., Hughes, G.W., 1981. Scanning laser ophthalmoscope. IEEE Trans. Biomed. Eng. (7) 488–492.

Welikala, R., Foster, P., Whincup, P., Rudnicka, A., Owen, C., Strachan, D., Barman, S., 2017. Automated arteriole and venule classification using deep learning for retinal images from the UK biobank cohort. Comput. Biol. Med. 90, 23–32. doi:10.1016/j.compbiomed.2017.09.005.

Winder, R.J., Morrow, P.J., McRitchie, I.N., Bailie, J., Hart, P.M., 2009. Algorithms for digital image processing in diabetic retinopathy. Computerized medical imaging and graphics 33 (8), 608–622.

Wong, T., Mitchell, P., 2007. The eye in hypertension. The Lancet 369 (9559), 425–435.

Wong, T.Y., Klein, R., Klein, B.E., Tielsch, J.M., Hubbard, L., Nieto, F.J., 2001. Retinal microvascular abnormalities and their relationship with hypertension, cardiovascular disease, and mortality. Surv. Ophthalmol. 46 (1), 59–80.

Wong, T.Y., Klein, R., Sharrett, A.R., Manolio, T.A., Hubbard, L.D., Marino, E.K., Kuller, L., Burke, G., Tracy, R.P., Polak, J.F., et al., 2003. The prevalence and risk factors of retinal microvascular abnormalities in older persons: the cardiovascular health study. Ophthalmology 110 (4), 658–666.

Wong, T.Y., Knudtson, M.D., Klein, R., Klein, B.E., Meuer, S.M., Hubbard, L.D., 2004. Computer-assisted measurement of retinal vessel diameters in the beaver dam eye study: methodology, correlation between eyes, and effect of refractive errors. Ophthalmology 111 (6), 1183–1190.

Wu, Y., Xia, Y., Song, Y., Zhang, Y., Cai, W., 2018. Multiscale network followed network model for retinal vessel segmentation. In: International Conference on Medical Image Computing and Computer-Assisted Intervention. Springer, pp. 119–126.

Xu, X., Ding, W., Abràmoff, M.D., Cao, R., 2017. An improved arteriovenous classification method for the early diagnostics of various diseases in retinal image. Comput. Methods Programs Biomed. 141, 3–9.

Xu, X., Tan, T., Xu, F., 2018. An improved u-net architecture for simultaneous arteriole and venule segmentation in fundus image. In: Annual Conference on Medical Image Understanding and Analysis. Springer, pp. 333–340.

Xue, L.-Y., Lin, J.-W., Cao, X.-R., Yu, L., 2018. Retinal blood vessel segmentation using saliency detection model and region optimization. Journal of Algorithms & Computational Technology 12 (1), 3–12.

Yan, Y., Wen, D., Dewan, M.A.A., Huang, W.-B., 2017. Classification of artery and vein in retinal fundus images based on the context-dependent features. In: International Conference on Digital Human Modeling and Applications in Health, Safety, Ergonomics and Risk Management. Springer, pp. 198–213.

Yan, Z., Yang, X., Cheng, K.-T., 2018. Joint segment-level and pixel-wise losses for deep learning based retinal vessel segmentation. IEEE Trans. Biomed. Eng. 65 (9), 1912–1923.

Yan, Z., Yang, X., Cheng, K.-T.T., 2018. A three-stage deep learning model for accurate retinal vessel segmentation. IEEE J. Biomed. Health Inform..

Yang, J., Dong, X., Hu, Y., Peng, Q., Tao, G., Ou, Y., Cai, H., Yang, X., 2020. Fully automatic arteriovenous segmentation in retinal images via topology-aware generative adversarial networks. Interdisciplinary Sciences: Computational Life Sciences 1–12.

Yang, X., Liu, C., Le Minh, H., Wang, Z., Chien, A., Cheng, K.-T.T., 2017. An automated method for accurate vessel segmentation. Physics in Medicine & Biology 62 (9), 3757.

Yau, J.W., Rogers, S.L., Kawasaki, R., Lamoureux, E.L., Kowalski, J.W., Bek, T., Chen, S.-J., Dekker, J.M., Fletcher, A., Grauslund, J., et al., 2012. Global prevalence and major risk factors of diabetic retinopathy. Diabetes Care DC_111909.

Yin, X., Irshad, S., Zhang, Y., 2020. Classifiers fusion for improved vessel recognition with application in quantification of generalized arteriolar narrowing. J. Innov. Opt. Health Sci. 13 (01), 1950021.

Zana, F., Klein, J.-C., 1999. A multimodal registration algorithm of eye fundus images using vessels detection and hough transform. IEEE Trans. Med. Imaging 18 (5), 419–428.

Zhang, B., Karray, F., Li, Q., Zhang, L., 2012. Sparse representation classifier for microaneurysm detection and retinal blood vessel extraction. Inf. Sci. (Ny) 200, 78–90.

Zhang, J., Chen, Y., Bekkers, E., Wang, M., Dashtbozorg, B., ter Haar Romeny, B.M., 2017. Retinal vessel delineation using a brain-inspired wavelet transform and random forest. Pattern Recognit. 69, 107–123.

Zhang, J., Dashtbozorg, B., Bekkers, E., Pluim, J.P., Duits, R., ter Haar Romeny, B.M., 2016. Robust retinal vessel segmentation via locally adaptive derivative frames in orientation scores. IEEE Trans. Med. Imaging 35 (12), 2631–2644.

Zhang, J., Li, H., Nie, Q., Cheng, L., 2014. A retinal vessel boundary tracking method based on bayesian theory and multi-scale line detection. Computerized Medical Imaging and Graphics 38 (6), 517–525.

Zhang, L., Fisher, M., Wang, W., 2015. Retinal vessel segmentation using multi-scale textons derived from keypoints. Computerized Medical Imaging and Graphics 45, 47–56.

Zhang, Y., Chung, A., 2018. Deep supervision with additional labels for retinal vessel segmentation task. arXiv preprint arXiv:1806.02132.

Zhao, H., Li, H., Maurer-Stroh, S., Cheng, L., 2018. Synthesizing retinal and neuronal images with generative adversarial nets. Med. Image Anal. 49, 14–26.

Zhao, Y., Liu, Y., Wu, X., Harding, S.P., Zheng, Y., 2015. Retinal vessel segmentation: an efficient graph cut approach with retinex and local phase. PLoS ONE 10 (4), e0122332.

Zhao, Y., Rada, L., Chen, K., Harding, S.P., Zheng, Y., et al., 2015. Automated vessel segmentation using infinite perimeter active contour model with hybrid region information with application to retinal images.. IEEE Trans. Med. Imaging 34 (9), 1797–1807.

Zhao, Y., Xie, J., Su, P., Zheng, Y., Liu, Y., Cheng, J., Liu, J., 2018. Retinal artery and vein classification via dominant sets clustering-based vascular topology estimation. In: International Conference on Medical Image Computing and Computer-Assisted Intervention. Springer, pp. 56–64.

Zhao, Y., Xie, J., Zhang, H., Zheng, Y., Zhao, Y., Qi, H., Zhao, Y., Su, P., Liu, J., Liu, Y., 2019. Retinal vascular network topology reconstruction and artery/vein classification via dominant set clustering. IEEE Trans. Med. Imaging 39 (2), 341–356.

Zhao, Y., Zhao, J., Yang, J., Liu, Y., Zhao, Y., Zheng, Y., Xia, L., Wang, Y., 2017. Saliency driven vasculature segmentation with infinite perimeter active contour model. Neurocomputing 259, 201–209.

Zhao, Y.Q., Wang, X.H., Wang, X.F., Shih, F.Y., 2014. Retinal vessels segmentation based on level set and region growing. Pattern Recognit. 47 (7), 2437–2446.

Zhen, Y., Gu, S., Meng, X., Zhang, X., Zheng, B., Wang, N., Pu, J., 2014. Automated identification of retinal vessels using a multiscale directional contrast quantification (mdcq) strategy. Med. Phys. 41 (9).

Zheng, Y., Hijazi, M.H.A., Coenen, F., 2012. Automated disease-no disease grading of age-related macular degeneration by an image mining approach. Investigative ophthalmology & visual science 53 (13), 8310–8318.

Zhou, L., Yu, Q., Xu, X., Gu, Y., Yang, J., 2017. Improving dense conditional random field for retinal vessel segmentation by discriminative feature learning and thin-vessel enhancement. Comput. Methods Programs Biomed. 148, 13–25. doi:10.1016/j.cmpb.2017.06.016.

Zhu, C., Zou, B., Xiang, Y., Cui, J., Wu, H., 2016. An ensemble retinal vessel segmentation based on supervised learning in fundus images. Chinese Journal of Electronics 25 (3), 503–511.

Zhu, C., Zou, B., Zhao, R., Cui, J., Duan, X., Chen, Z., Liang, Y., 2017. Retinal vessel segmentation in colour fundus images using extreme learning machine. Computerized Medical Imaging and Graphics 55, 68–77.

Zou, B.-J., Chen, Y., Zhu, C.-Z., Chen, Z.-L., Zhang, Z.-Q., 2017. Supervised vessels classification based on feature selection. J. Comput. Sci. Technol. 32 (6), 1222–1230.